Marine Environmental Research
September 2022, Volume 180, Pages 105709 (14p.)
https://doi.org/10.1016/j.marenvres.2022.105709
https://archimer.ifremer.fr/doc/00787/89883/

Archimer
https://archimer.ifremer.fr

Harsh intertidal environment enhances metabolism and immunity in oyster (*Crassostrea gigas*) spat

Corporeau Charlotte [1, *], Petton Sébastien [1], Vilaça Romain [1], Delisle Lizenn [1], Quéré Claudie [1], Le Roy Valerian [1], Dubreuil Christine [1], Lacas-Gervais Sandra, Guitton Yann [3], Artigaud Sebastien [1], Bernay Benoît [4], Pichereau Vianney [1], Huvet Arnaud [1], Petton Bruno [1], Pernet Fabrice [1], Fleury Elodie [1], Madec Stephanie [1], Brigaudeau Christophe [5], Brenner Catherine [6], Mazure Nathalie M. [7]

[1] Ifremer, Univ. Bretagne Occidentale, CNRS, IRD, Équipe soutenue par la fondation ARC, UMR 6539, LEMAR, F, 29280, Plouzané, France
[2] Université Côte d'Azur, Centre Commun de Microscopie Appliquée, CCMA, Nice, France
[3] Laboratoire d'étude des Résidus et Contaminants dans les Aliments, Oniris, INRA, F-44307, Nantes, France
[4] Plateforme Proteogen, SFR ICORE 4206, Univ. Caen Basse-Normandie, 14000, Caen, France
[5] Inserm U1227, Univ. Bretagne Occidentale, 2 bis avenue Foch, 29200, Brest, France
[6] Université Paris-Saclay, CNRS, Institut Gustave Roussy, Aspects métaboliques et systémiques de l'oncogénèse pour de nouvelles approches Thérapeutiques, 94805, Villejuif, France
[7] Inserm U1065, Centre Méditerranéen de Médecine Moléculaire, 151 route St Antoine de Ginestière, 06204, Nice, France

* Corresponding author : Charlotte Corporeau, email address : charlotte.corporeau@ifremer.fr

Abstract :

The Pacific oyster Crassostrea gigas is established in the marine intertidal zone, experiencing rapid and highly dynamic environmental changes throughout the tidal cycle. Depending on the bathymetry, oysters face oxygen deprivation, lack of nutrients, and high changes in temperature during alternation of the cycles of emersion/immersion. Here we showed that intertidal oysters at a bathymetry level of 3 and 5 m delayed by ten days the onset of mortality associated with Pacific Oyster Mortality Syndrome (POMS) as compared to subtidal oysters. Intertidal oysters presented a lower growth but similar energetic reserves to subtidal oysters but induced proteomic changes indicative of a boost in metabolism, inflammation, and innate immunity that may have improved their resistance during infection with the Ostreid herpes virus. Our work highlights that intertidal harsh environmental conditions modify host-pathogen interaction and improve oyster health. This study opens new perspectives on oyster farming for mitigation strategies based on tidal height.

Please note that this is an author-produced PDF of an article accepted for publication following peer review. The definitive publisher-authenticated version is available on the publisher Web site.

Graphical abstract

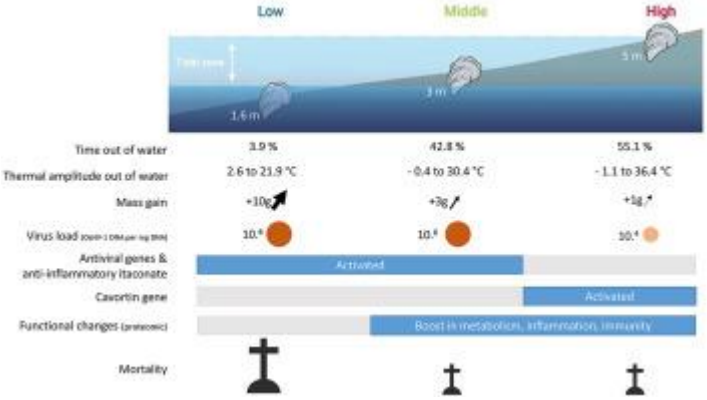

Highlights

► The metabolism and immunity of oysters are modified as a function of their habitat. ► Increasing oysters' bathymetry is an advantage against pathogens in the field. ► An intertidal footprint in oysters is detected at the proteomic level.

Keywords : environment, marine invertebrate, metabolism, OsHV-1

Please note that this is an author-produced PDF of an article accepted for publication following peer review. The definitive publisher-authenticated version is available on the publisher Web site.

1. INTRODUCTION

The Pacific oyster *Crassostrea gigas* (*C. gigas*) is a sessile estuarine bivalve living in the coastal zone. *C. gigas* constitutes a great model species able to support rapid and dynamic environmental changes. Intertidal oysters are daily exposed to rapid changes in the food supply, oxygen, salinity, pH, and temperature conditions, throughout the tidal cycle depending on their bathymetric level (Li et al., 2018; Scanes et al., 2017; Zhang et al., 2016, 2012). *C. gigas* endures temperatures ranging from below zero to 49°C, salinities from 10 up to 35 ppm and is particularly well adapted to anoxia during prolonged air exposure as well as rapid and long-term hypoxia (0.1% O_2; weeks to months) (Bayne, 2017; Donaghy et al., 2013; Falfushynska et al., 2020; Guévélou et al., 2013; Sussarellu et al., 2013, 2012). In contrast to vertebrates, *C. gigas* presents an exceptional mitochondrial resilience to temperature, salinity, hypoxia (Sokolova, 2018), and extreme tolerance to hypoxia was related to mitochondria plasticity ability to maintain respiratory capacity in response to oxygen loss (Donaghy et al., 2013; Sokolov et al., 2019; Sussarellu et al., 2013, 2012). *C. gigas* can survive fasting for more than 6 months at 14°C (Whyte et al., 1990) and continue sexual maturation under complete food deprivation at 18°C (Rozenn Cannuel, 2005). *C. gigas* possesses unique molecular features to respond to environmental changes in its intertidal stressful habitat, based on a combination of

strong cellular homeostasis control, a large number of chaperone heat-shock hsp70 genes (88), and several copies of anti-oxidant enzymes (Zhang et al., 2016, 2012). The intertidal Pacific oyster is therefore a good model species to study the interaction between physical traits of a stressful intertidal environment and biological regulation of cellular energetic metabolism.

Since 2008, spat oysters are dying in most rearing areas in the world. Mortality results from a Pacific Oyster Mortality Syndrome (POMS) caused by the Ostreid Herpes Virus-1 (OsHV-1) infection and followed by fatal bacteremia (de Lorgeril et al., 2018). OsHV-1 replicates in oyster circulating immune cells (hemocytes) which induces an immune depression and subsequent bacterial colonization leading to death (de Lorgeril et al., 2018; Morga et al., 2017). Oyster metabolism is a key component of POMS since the energy metabolism is highjacked by OsHV-1 for its replication, as the viral appropriation of host-cell biomaterials. Indeed, as shown in *C. gigas* larvae, OsHV-1 induces a metabolic reprogramming known as the Warburg effect (Corporeau et al., 2019, 2014; Rosani et al., 2019; Sanchez and Lagunoff, 2015; Young et al., 2017). The Warburg effect could facilitate the creation of new OsHV-1 viral particles in *C. gigas* during its replication phase, as demonstrated in *Paeneus japonicus* shrimp during infection by the white spot syndrome virus (WSSV) (Chen et al., 2011; Su et al., 2014). The Warburg effect is a metabolic reprogramming of cells producing large amounts of building blocks (DNA, lipids, amino acids) for division, which is one hallmark of proliferating cancer cells in vertebrates (Fouad and Aanei, 2017; Warburg, 1956).

Interestingly, increasing the bathymetry of oyster settlements decreases the mortality risk during an OsHV-1 outbreak (Azéma et al., 2017; Pernet et al., 2019) but mechanisms remain unknown. Here we deployed oysters in a farming area at Low (1.6 m; subtidal), Middle (3 m; intertidal), and High (5 m; intertidal) bathymetry corresponding to 3.9% (subtidal), 42.8%, and 55.1% (intertidal) emersion time, respectively. We monitored local temperature in the bag and analyzed the physiological responses of oysters during OsHV-1-associated mortality as a function of the bathymetry. We analyzed the impact of bathymetry on oyster physiology by using “omics” technologies (proteomics and metabolomics) referenced as emergent tools for the study of host-pathogen interaction in bivalves and to identify bioindicators of animal health (Alfaro and Young, 2018; Rosani et al., 2019). To identify any changes in interaction with OsHV-1, we quantified OsHV-1 DNA in oysters, used electronic microscopy to observe cell phenotypes, and studied gene, proteomic and metabolic responses during the disease outbreak. Our results revealed that a harsh fluctuating environment boosts metabolism, inflammation, and immunity in oysters, promoting resistance to POMS. It involves some changes in the mitochondrial functioning and results in delayed mortality for intertidal oysters.

2. MATERIALS AND METHODS

2.1 *Experimental design*

Specific-pathogen free oyster (SPF) spats were produced at Ifremer's laboratory (France; (Petton et al., 2015) and maintained in a hatchery. They were deployed on the 2nd of March 2018 in an experimental site with oyster farming in the Bay of Brest (Brittany, France, 48° 20′ 06.19″ N, 4° 19′ 06.37″ W) that belongs to the oyster observatory network ECOSCOPA (Fleury et al., 2021). The 6 months-old SPF (mean size of ~1.2 cm; mean weight of ~1.5 g) were placed in regular-sized mesh oyster bags (length: 1 m; width: 0,3 m; mesh: 9 mm diameter) and the density was 300 oysters per bag (total biomass = 450 g per bag) according to standard rearing procedures (Fleury et al., 2020). The bags were deployed at three bathymetric levels (3 bags per bathymetry; 9 bags in total) in the natural limits of wild *C. gigas* repartition in the field: Low =1.6 m above Chart Datum (+CD; subtidal); Middle =3 m +CD (intertidal); High =5 m +CD (intertidal). Oysters were sampled on 14th May 2018. They were counted and weighed every 15 days until the end of the experiment (13th of July) to monitor growth and mortality, according to the protocol described by the RESCO network (Mazaleyrat et al., 2022).

2.2 ***In situ*** **temperature and pressure data monitoring**

Autonomous data loggers (SP2T© from NKE, Hennebont, France) were used to monitor temperature and pressure for oysters at each studied bathymetry (one logger per level) with a record of one data per minute. Immersion time relative to the total submerged tracking time was calculated with pressure data. The maximum permissible deviation allowed for temperature data was ± 0.1°C. We calculated the time spent ≥ 16°C in seawater, ≥ 24°C, and ≥ 29°C in air, using the number of days multiplied by the temperature of 16°C, 24°C, or 29°C (expressed in °C.day). Datasets of *in situ* temperature and pressure are available at DOI: 10.17882/79095 (Petton et al., 2020).

2.3 **Sample preparation**

On 14th May 2018, 25 oysters per bag were sampled (25 oysters x 3 bags x 3 bathymetric levels; 9 bags in total). In each bag, 10 oysters were sampled for OsHV-1 DNA quantification (n=10 biological samples per bag) and among them, 5 were used for gene expression (n=5 biological samples per bag) and 5 samples were pooled for biochemical analyses, proteomics and LC-HRMS metabolomics (n= 1 pool of 5 individuals per bag). In addition, 10 oysters were sampled in each bag for extraction of the mitochondrial-enriched fraction before nano-LC MS/MS proteomic analysis (n= 1 pool of 10 individuals per bag). Then, 5 oysters were sampled in each bag to dissect the heart for transmission electron microscopy (TEM). All the analyses were done in triplicates (n= 3 technical replicates).

2.4 **OsHV-1 DNA quantification**

Oyster's flesh (n=10 individuals per bag x 3 bags x 3 bathymetric levels) was frozen in liquid nitrogen after removing the shells, then grounded using an MM400 homogenizer (Retsch, Eragny, France). OsHV-1 DNA quantification was conducted by LABOCEA (Brest, France) on total DNA (n=10) extracted with a QIAamp tissue mini kit (Qiagen, Hilden, Germany) according to (Pepin et al., 2008). The extract was stored at −20 °C before detection and quantification according to a real-time PCR protocol based on SYBR Green chemistry with specific primers (Webb et al., 2007). Results were expressed as the log (OsHV-1 DNA copy) per mg of total DNA.

2.5 **Transmission electronic microscopy (TEM)**

The heart, one of the tissues targeted by OsHV-1 (Segarra et al., 2014), was sampled from live oysters (n=10 per bag) and fixed for 2 h in glutaraldehyde 2.5% diluted in cacodylate buffer 0.1M pH 7.4. The remaining oyster flesh was kept for further quantification of OsHV-1 DNA (data not shown). The obtained values of OsHV-1 DNA were used to assign the infection status of the oyster to TEM pictures. Hearts were rinsed in 0.1 M cacodylate buffer and post-fixed for 2 h in a solution of 1% osmium tetroxide, 1% potassium ferrocyanide in 0.1 M cacodylate buffer to enhance the staining of membranes, rinsed in distilled water, dehydrated in acetone, then embedded in epoxy resin using an automat Leica EM AMW. Contrasted ultrathin sections (70 nm) were analyzed under a JEOL 1400 transmission electron microscope mounted with a Morada CCD camera (Olympus, Rungis, France).

2.6 **Gene expression analysis**

Powder of oysters among those used for OsHV-1 DNA (5 individuals per bag x 3 bags x 3 bathymetric levels; 30 mg each) was used for total RNA isolation using 1.5 mL of Extract-all (Eurobio, Courtaboeuf, France) and extracted with phenol-chloroform according to the manufacturer's instructions. RNA pellets diluted in molecular biology quality water were treated with DNase (DNase Max™ Kit; Thermo Fisher Scientific, Les Ulis, France) using 1 U. μg^{-1} total RNA to remove genomic DNA. Quality and quantity of RNA were determined using a NanoDrop 2000 (Thermo Fisher Scientific, Les Ulis, France) and a Bioanalyser 2100 (Agilent; Santa Clara, CA, USA) with RNA nano chips (Sussarellu et al., 2016). To verify the absence of DNA carryover, RNA samples were 1:10 diluted and analyzed in real-time PCR using elongation factor 1 primers (**Table 1**). First-strand cDNA synthesis was performed using the iScript™ cDNA Synthesis Kit (Bio-rad; Marnes-la coquette, France) with 1 µg RNA. We analyzed the relative expression of four genes (**Table 1**): inhibitor of apoptosis *IAP* (regulation of cell survival and cell-death processes), *an* inhibitor of kappa Beta 2 *IKB2* (propagation of

the cellular response to inflammation), protein kinase RNA-activated *PKR* (a potent mediator of antiviral effects exerted by interferons) and Cavortin *CAV (or EcSOD,* an Extracellular Superoxide Dismutase involved in antioxidant response*)*. Real-time PCR was performed in triplicate with 5 µL cDNA (1/20) in 15 µL with final concentrations of 0.2 µM each primer, and 1 X SSo Advanced Universal SYBR Green Supermix (Bio-rad; Marnes-la coquette, France). Cycling conditions were: activation at 95 °C for 5 min followed by 40 cycles of 10 sec at 95 °C, 20 sec at 60 °C, and a melting curve program from 69 to 95 °C by increasing the temperature by 0.5 °C every 10 sec. Each run included a pool of cDNA as a positive control (used as calibrator) and blank controls (water) for each primer pair. PCR efficiency ($E = 10^{(-1/slope)}$) was determined by drawing standard curves from a serial dilution of the calibrator to ensure that E ranged from 90% to 110% for each primer pair. The relative mRNA levels were calculated based on a comparative Ct method (Livak and Schmittgen, 2001). No difference between Ct values was observed for the gene *MnSOD.* Therefore, the relative quantification values of samples were normalized with *MnSOD* level and relative to the calibrator, and were expressed in arbitrary units as $2^{-\Delta\Delta Cq}$ with ΔCq = Cq (studied gene) – Cq (*MnSOD*) and $\Delta\Delta Cq = \Delta Cq$ of cDNA sample – ΔCq of the cDNA calibrator.

Table 1. Sequences and characteristics of primers used for real-time PCR analyses. Forward (F) or reverse (R) primer, nucleotide sequence, product size of the amplicon (bp), and efficiency of the primer pair (E). The original publication of each EST/mRNA is given.

Gene name	Ensembl gene ID / Genbank #	ID	F/R	Sequence 5'- 3'	Product size	E (%)	Reference
Inhibitor of apoptosis	XM_034479730	IAP	F	CCCGAAAACGTAACCTCAGA	287	99.3	Segarra et al 2014
			R	TTTCGTTTGCTGCTCATTTG			
NF-kappa-B Inhibitor 2	AM856743	IKB2	F	CAGCATTCACTGACGACGAT	165	100.1	Zhang et al 2011
			R	TCTGCCTCAGTTTGTCGTTG			
Eukaryotic translation initiation factor 2-alpha kinase	XM_034478602	PKR (EIF2AK)	F	GTAGCACCAGGAGATGGTTC	130	99	Namely PKR in Green & Montagnani 2013
			R	GAGCATCAGCAAAGTGTTGAG			
Cavortin (Extracellular superoxide dismutase)	CU681762	CAV (EcSOD)	F	CTTCATGCCAGGCAACCT	107	101.4	Gonzalez et al 2005
			R	TGACGTTGAATCCGGTCA			
Manganese superoxide dismutase	CU681620	MnSOD	F	AGTCTGGTCGCACATTCTTGT	111	101.4	Park et al 2009
			R	CATGTGCCAATCAAGATCCTC			
Elongation factor 1	BQ426516	EF1	F	GATTGCCACACTGCTCACAT	104	100	Fabioux et al 2004
			R	AGCATCTCCGTTCTTGATGC			

2.7 **LC-HRMS metabolomic analysis**

Powder of oysters among those used for OsHV-1 DNA (5 individuals per bag; 20 mg each) was pooled (1 pool x 3 bags x 3 bathymetric levels) and extracted in 1.4 ml of MeOH, vortexed 20 sec, put in an ultrasonic bath for 10 min, and centrifuged 2 min (4000 rpm, 20°C). Two different LC-HRMS approaches were applied in this study, namely Reverse Phase-Metabolomics (RP-metabolomics) targeting semi-polar metabolites, and HILIC Phase-Metabolomics (HILIC-Metabolomics) for polar metabolites (Cesbron et al., 2017). For RP-metabolomics, 300 µl supernatant was dried under nitrogen and reconstituted in 50 µl Water/MeCN (5/95). Chromatographic separation was performed on the Hypersil GOLD C18 column (1.9 µm particle size, 100 x 2.1 mm) and was achieved using a mobile phase of (A) water/acetonitrile (95/5 w/v) and (B) acetonitrile/water (95/5) each containing 0.1% acetic acid. The gradient elution was 0-2.40 min, 25% B; 2.40-4.50 min, 70% B; 4.50-11 min, 100% B with a hold for 3 min; 14-16.5 min, linear decrease to 5% B then hold for 3.5 min. All sample fingerprinting was performed on a Thermo Ultimate3000 HPLC system coupled to a Finnigan hybrid mass spectrometer (QExactive, Thermo Fisher Scientific, Les Ulis, France). The column temperature was set at 35°C with an LC flow of 0.4 mL/min, the vial rack temperature at 10°C, and the injection volume was 5 µL. Then, a heated electrospray ionization source (H-ESI) was used in polarity switch mode with the voltage set to -3.00 kV in negative mode and 3.00 kV in positive mode. The capillary voltage was set to 30 V and the tube lens offset to 100 V. The sheath and auxiliary gas flows were set to 55 and 6 arbitrary units, respectively, and the drying gas temperature was set to 350 °C. Mass spectra were recorded from m/z 65.0 to m/z 975.0 at a resolving power of 35000 Full-Width Half Maximum (FWHM) measured at m/z 200. The Automatic Gain Control (AGC target) was set at a high dynamic range (5×10^5) with a 100 ms maximum injection time. MS instrument external calibrations were performed using the Calmix-positive and Calmix-negative standard solutions for the positive and the negative ionization modes, respectively. For HILIC-metabolomics, 590 µl were dried under nitrogen and reconstituted in 100 µl of 90/10 acetonitrile/Water. Chromatographic separation was performed on a SeQuant ZIC-HILIC 5 µm, 200 Å 150 x 2.1 mm (Merck KGaA, Gernsheim, Germany) and achieved using a mobile phase of (A) 10 mM ammonium acetate (pH 4.75) in water and (B) acetonitrile containing 10 mM Ammonium acetate and 1% water (pH 4.75). The used elution gradient (A:B, v/v) was as follows: 5:95 from 0 to 2 min; 20:80 at 5 min; 40:60 at 12 min; 60:40 at 14 min to 16 min; 5:95 at 18 to 28 min. A pooled quality control (QC) sample was prepared to ensure that no or minimal metabolic information was lost and for system equilibration. QC samples were extracted along with each sample batch and analyzed

throughout the analytical run, to provide robust quality assurance. Every injection vial was spiked with 1ng/µl of internal standards (L-Leucine-5,5,5-d3, L-Tryptophan-2,3,3-d3, Indole-2,4,5,6,7-d5-3-acetic acid and 1,14-Tetradecanedioic-d24 acid). Acquisitions were made on a Thermo Ultimate3000 HPLC system coupled to a Finnigan hybrid mass spectrometer (QExactive, Thermo Fisher Scientific, Les Ulis, France). MSCAL6 ProteoMass LTQ/FT-Hybrid, MS instrument calibration standard mixtures, were obtained from Sigma-Aldrich (Saint Quentin Fallavier, France). LC-MS metabolomics data (LC-MS negative mode data for itaconate) are available at https://www.ebi.ac.uk/metabolights/MTBLS2475.

2.8 **Nano-LC MS/MS proteomic analysis of mitochondrial-enriched fraction**

The flesh of ten individuals per bag (10 individuals x 3 bags x 3 bathymetric levels) was used for isolation of mitochondrial-enriched protein extract adapted from (Wang et al., 2016). The flesh of 10 oysters was dried by dabbing on a paper tissue, weighed, and rinsed on 80 µm mesh with 1 ml isolation buffer containing 300 mM sucrose, 5 mM TES, 200 mM EGTA, with antiproteases added extemporaneously (Complete™ Protease Inhibitor Cocktail, Sigma-Aldrich; Saint Quentin Fallavier, France), pH 7.2. The flesh was then chopped with scissors and homogenized in the ice-cold isolation buffer at a 1/3 mass volume ratio first slightly in a motorized Potter tissue grinder (Heidolph, 153 Kelheim, Germany), then by 10 passes in a Dounce homogenizer. Homogenate was filtered on 80 µm mesh and centrifuged at 900 g at 4°C for 10 min to remove cellular debris. The supernatant was collected, filtered again on 80 µm mesh, and centrifuged at 9,000 g at 4°C for 10 min. The mitochondrial pellet was re-suspended in 400 µl of ice-cold protein extraction buffer containing 50 mM Bis-Tris, 750 mM aminocaproic acid, 1% (m/v) n-dodecyl-β-D-maltopyranoside, with antiproteases added extemporaneously (Complete™ Protease Inhibitor Cocktail, Sigma-Aldrich; Saint Quentin Fallavier, France), pH 7. Proteins were solubilized overnight at 4°C using a rotary stirrer, then extracted by centrifugation at 10,000 g for 45 min at 4°C. Protein extracts were homogenized in concentration then reduced (50 mM DTT) and alkylated (55 mM Iodoacetamide) before overnight trypsin digestion at 37°C. For nano-LC fragmentation, protein or peptide samples were desalted and concentrated onto a µC18 Omix (Agilent; Santa Clara, CA, USA). The chromatography step was performed on a NanoElute (Bruker Daltonics; Bremen, Germany) ultra-high pressure nanoflow chromatography system. Peptide samples were concentrated onto a C18 pepmap 100 (5 mm x 300 µm i.d.) precolumn (Thermo Fisher Scientific, Les Ulis, France) and separated at 50°C onto a reversed-phase Reprosil column (25 cm x 75 µm i.d.) packed with 1.6 µm C18 coated porous silica beads (Ionopticks; Fitzroy, Australia). Mobile phases consisted of 0.1% formic acid, 99.9% water (v/v) (A) and 0.1% formic acid in 99.9%

acetonitrile (v/v) (B). The nanoflow rate was set at 400 nl/min, and the gradient profile was: 2 to 15% B (60 min), increase to 25% B (30 min), 37% B (10 min), washing step at 95% B, re-equilibration. MS experiments were carried out on a TIMS-TOF pro mass spectrometer (Bruker Daltonics; Bremen, Germany) with a modified nanoelectrospray ion source (CaptiveSpray, Bruker Daltonics; Bremen, Germany). The system was calibrated each week and mass precision was better than 1 ppm. A 1400 spray voltage with a capillary temperature of 180°C was typically employed for ionizing. MS spectra were acquired in the positive mode in the mass range from 100 to 1700 m/z. The mass spectrometer was operated in PASEF mode with the exclusion of single charged peptides and 10 PASEF MS/MS scans were performed during 1.25 sec from charge range 2-5. The fragmentation pattern was used to determine the sequence of the peptide. Database searching was performed using the Peaks X software. A Uniprot *Crassostrea gigas* database was used. The variable modifications allowed were as follows: C-Carbamidomethylation, K-acetylation, and methionine oxidation. "Trypsin" was selected as semispecific. Mass accuracy was set to 30 ppm and 0.05 Da for MS and MS/MS modes respectively. Data were filtered according to an FDR of 0.5%, two unique peptides, and protein redundancy elimination based on proteins being evidenced by the same set or a subset of peptides. To quantify the relative protein abundance levels between groups, three technical replications of each sample (nine LC-MS/MS runs) were analyzed using the label-free quantification feature of PEAKS X+ software. Feature detection was separately performed on each sample by the expectation-maximization-based algorithm. The features of the same peptide from all samples were aligned through the retention time alignment algorithms. Mass error tolerance was set at 30 ppm and retention time tolerance at 10 min. Samples normalization factors were obtained by the total ion current (TIC) of each sample/the TIC of the reference sample which was automatically chosen by PEAKS. Protein abundance was calculated using the sum area of the top three unique peptides. Technical repeats of each sample were merged to give a protein detection profile. The protein abundance levels were separately compared for biological replicates. A 1.5-fold increase in relative abundance and a significance ≥ 10 using ANOVA were used to determine enriched proteins. In addition, quality was set >2, peptides must be detected in the least 2 samples per group and modified forms were excluded. The mass spectrometry proteomics data have been deposited to the ProteomeXchange Consortium via the PRIDE (Perez-Riverol et al., 2019) partner repository with the dataset identifier PXD025533.

2.9 **Statistical analyses**

The survival curves of oysters were compared among bathymetry using the Cox regression model. The proportionality of hazards (PH) was checked with martingale residuals (LIN et al.,

1993). Because the PH assumption was violated, time-dependent covariates representing the interaction of the bathymetry and log time were added to the model. Analyses were conducted using the SAS software package (SAS 9.4, SAS Institute). Kruskal-Wallis test was conducted to determine differences in OsHV-1 DNA in oyster tissues at each bathymetry. For other analyses, the normal distribution of data was checked by the Shapiro test, and the homogeneity of variances was evaluated using Bartlett's test. One-way ANOVA was done for gene expression data and targeted metabolomics and Tukey's HSD was used as a post hoc test to analyze relative gene expression and metabolomics according to the bathymetry. When necessary, data were log-transformed.

3. RESULTS

3.1 Environmental and oyster parameters

We analyzed the environmental conditions supported by oysters in the field until the onset of first mortalities in subtidal oysters at Low bathymetry on the 14th of May (**Fig. 1**). Subtidal oysters at Low bathymetry (1.6 m) presented 3.9% time of air exposure while intertidal oysters at the Middle (3 m) and High (5 m) bathymetry presented 42.8% or 55.1% time of air exposure, respectively (**Table 2**). High-frequency data indicated that the seawater temperature reached 16°C on the 4th of May (Low, Middle) and the 21st of April (High). Sixteen degrees corresponds to the minimal seawater temperature required for optimal disease spread and subsequent mortalities in the field (Pernet et al., 2018). Intertidal oysters at Middle and High reached aerial temperatures above 24°C and 29°C before the 14th of May, the date of sampling (**Table 2**). And oysters at High, the upper limit of *C. gigas* natural repartition, faced extreme aerial temperatures ranging from -1.1°C to 36.4°C during emersion. The mortality rates achieved by oysters on the 14th of May at the different bathymetry was 31.2% at Low in contrast to 0% at Middle and High in intertidal oysters.

Figure 1. Temperature profiles as a function of bathymetry. Temperature (°C) profiles until the sampling date (14th of May 2018) were obtained for oysters at Low (1,6m) Middle (3 m) and High (5m) bathymetric levels by using autonomous sensors (NKE ©) attached inside oyster bags. Data was tagged in blue during immersion (T°C Water) and green during emersion (T°C Air).

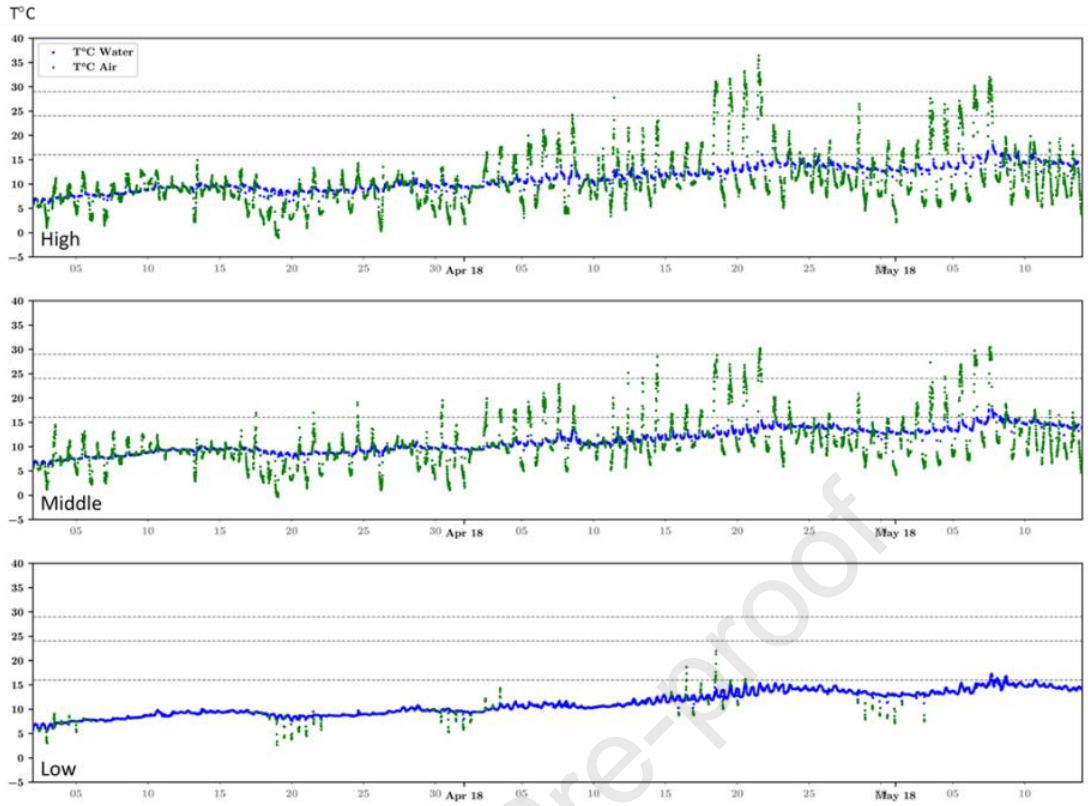

Table 2. Environmental characteristics experienced from the 2nd of March to the 14th of May (sampling date) by oysters at Low (1,6 m), Middle (3 m), and High (5 m) bathymetry: emersion and immersion duration (% time), temperature (°C min; °C max), time passed above 16°C, 24°C and 29°C (expressed as °C.day). Data sets are available at DOI: 10.17882/79095. Cumulative mortality of oysters at the sampling date is indicated (%).

	Emersion			Immersion			°C.day ≥16°C (water)	°C.day ≥24°C (air)	°C.day ≥29°C (air)	Mortality on 14th May (%)
	duration (%)	°C min	°C max	duration (%)	°C min	°C max				
High (5 m)	55.1	-1.1	36.4	44.9	5.9	18.1	0.25	7.69	1.42	0
Middle (3 m)	42.8	-0.4	30.4	57.2	5.9	17.7	0.26	3.23	0.11	0
Low (1.6 m)	3.9	2.6	21.9	96.1	5.7	17.2	0.25	0	0	31.2

3.2 **Energetic reserves, growth, survival, and OsHV-1 DNA amount**

Intertidal oysters at Middle and High bathymetry lowered their growth as compared to subtidal oysters at Low (**Fig. 2A).** The relative amount of energetic reserves (Carbohydrates, triacylglycerol/sterol and total protein) was similar in oysters at Low, Middle and High bathymetry (**Appendix Table A.1**). Mortalities occurred ten days earlier in subtidal oysters at Low compared to intertidal ones at Middle and High bathymetry (**Fig. 2B)**. At the onset of mortalities, on the 14th May, all animals were infected: the level of OsHV-1 DNA was above 10^5 copy per mg at Low and Middle bathymetry, but below 10^2 copy per mg in the High bathymetry conditions, except in two individuals with $\geq 10^5$ copy per mg (**Fig. 2C**). At the end

of our experiment, the final survival rate was lightly but statistically increased in intertidal oysters to 57% at Middle and 48% at High bathymetry, as compared to subtidal oysters with 41% survival rate at Low bathymetry (**Fig. 2B)**.

Figure 2. Ecophysiological parameters of oysters. (**A**) Body mass (g) and (**B**) survival (%) of oysters (n=300) at Low (1,6 m; blue), Middle (3 m; green) and High (5 m; red) bathymetry. (**C**) Quantification of OsHV-1 DNA on the 14th of May; n= 30 individuals per bathymetry; data were log (x+1) transformed and expressed as the log (OsHV-1 DNA copy) per mg of total DNA.

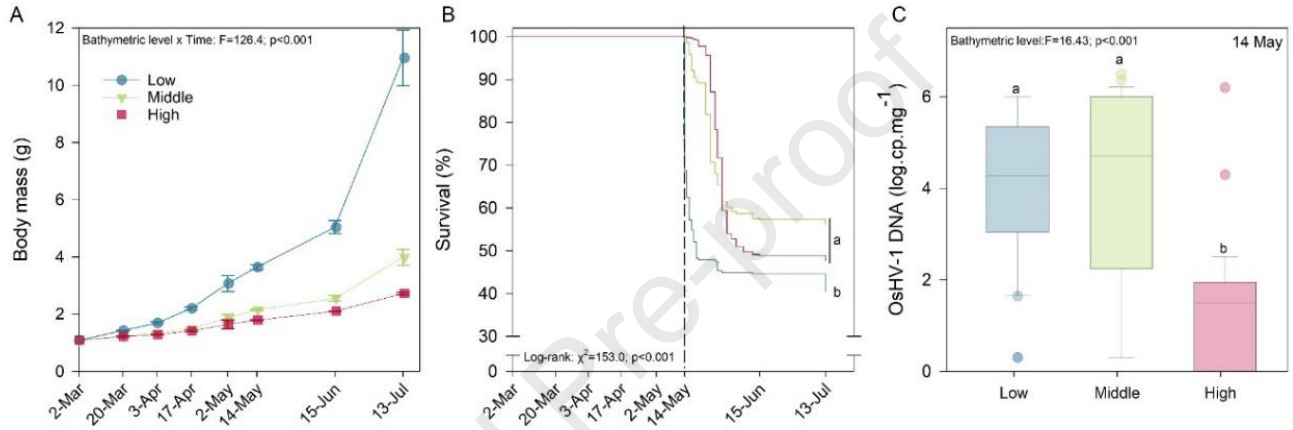

3.3 **Ultrastructural modifications of heart cells**

Transmission electronic microscopy (TEM) evidenced numerous lysosomes in heart cells in oysters at Low and Middle bathymetry, suggesting a higher lysosomal activity in oysters that presented a high level of OsHV-1 DNA (**Fig. 3**). In contrast, oysters at High bathymetry presented clear and rounded mitochondria as well as glycogen stored in rosettes.

Figure 3. Transmission Electronic microscopy analyses. TEM pictures of cardiomyocytes in oysters (n=4 per bathymetry) at Low (1,6 m), Middle (3 m), and High (5 m) bathymetry on the 14th of May. Green arrows show lysosomes, black arrows show glycogen stocks; (m) mitochondria; size is indicated with ladder lower right.

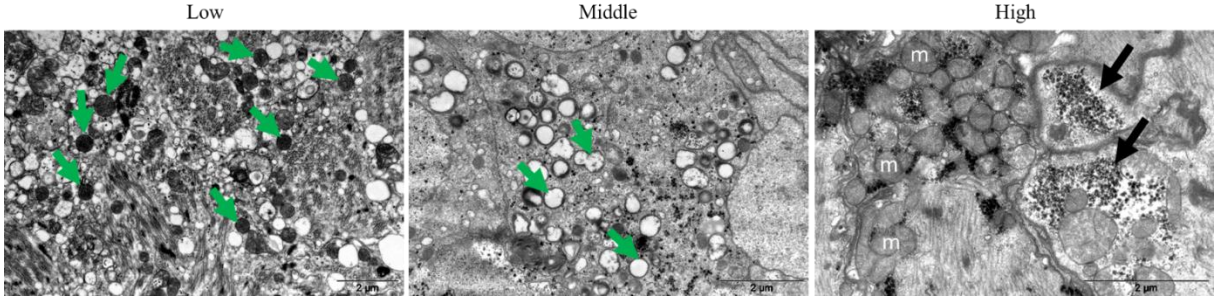

3.4 **Relative expression of immune-genes *IAP, IKB2, PKR,* and *CAV***

Oysters at Low and Middle bathymetry presented a high amount of *Cg IAP*, *Cg IKB2*, and *Cg PKR* mRNA (**Fig. 4).** These genes are involved in the anti-viral response of *C. gigas* to OsHV-1 (Pauletto et al., 2017). Our results showed that oysters at High bathymetry presented an important amount of *Cg CAV* mRNA while they had a low viral load. The cavortin *Cg CAV* encodes for the major protein secreted in response to stress in the hemolymph of *C. gigas* and is involved in defense against bacteria (Green et al., 2014; Itoh et al., 2011; Scotti et al., 2007). A correlative approach revealed that *Cg CAV* gene expression was negatively correlated to OsHV-1 DNA quantity (Pearson's r = - 0.42; pvalue = 0.0214; **Table 3).**

Figure 4. Immune gene expression. Relative expression of *Cg IAP, Cg IKB2, Cg PKR, and Cg CAV* in oysters (n=5 per level) at Low (1,6 m), Middle (3 m), and High (5 m) bathymetry. Data are expressed in arbitrary units relative to the *MnSOD* transcript level, as mean ± SEM (**p<0.1; ***p<0.01).

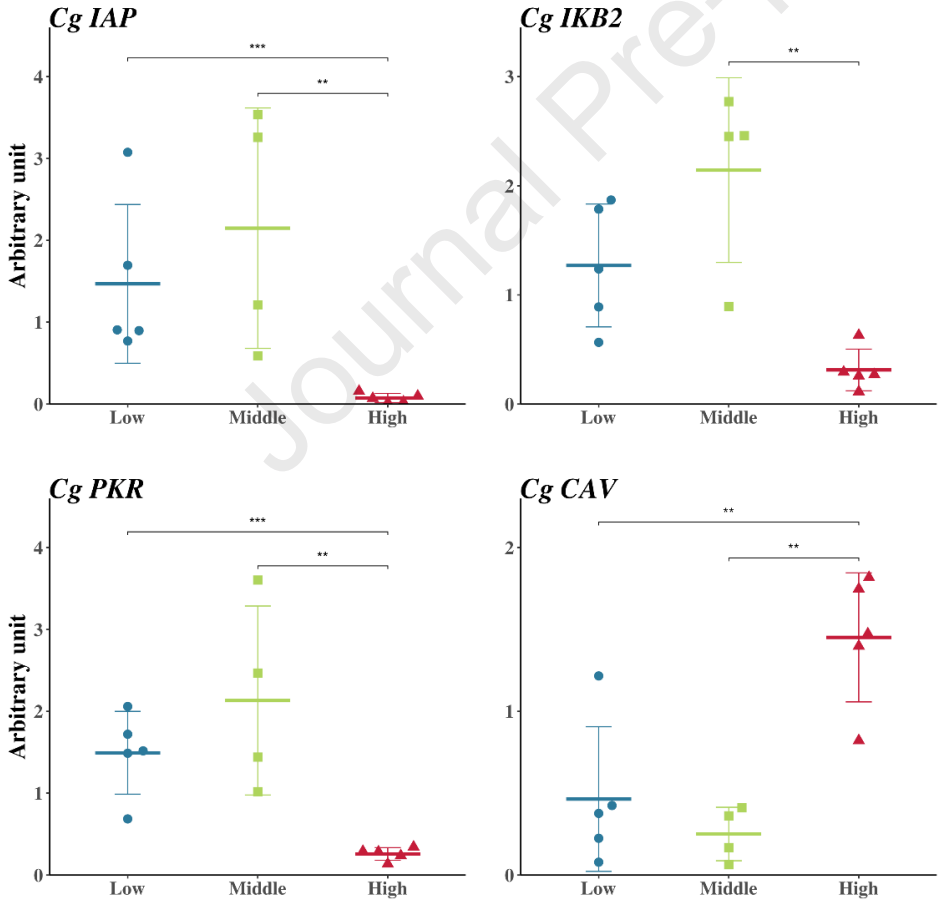

Journal Pre-proof

364 **Table 3.** Individual molecular data of *Cg CAV* mRNA (relative expression expressed in
365 arbitrary units relative to the *MnSOD* transcript level) and OsHV-1 DNA (copy per mg of total
366 DNA) used for the correlative study.

	Bathymetry	*Cg CAV* mRNA	OsHV-1 DNA
N51	Low	0.42	$2.27 \cdot 10^5$
N52	Low	0.08	$2.26 \cdot 10^5$
N53	Low	0.38	$7.72 \cdot 10^5$
N48B	Low	0.22	$1 \cdot 10^6$
N55B	Low	1.22	$1 \cdot 10^6$
N73B	Middle	1.67	$6.15 \cdot 10^3$
N65	Middle	0.36	$1.71 \cdot 10^6$
N71	Middle	0.06	$1.64 \cdot 10^6$
N72	Middle	0.17	$1.08 \cdot 10^6$
N75	Middle	0.41	$2.30 \cdot 10^6$
N76	High	1.47	$4.94 \cdot 10^1$
N79	High	1.82	$6.06 \cdot 10^1$
N80	High	1.75	$2.66 \cdot 10^1$
N82	High	0.82	$6.12 \cdot 10^1$
N89	High	1.40	$3.21 \cdot 10^1$

367 3.5 **Itaconate relative amount**

368 Metabolomic analyses identified statistical changes in the level of itaconate, an anti-
369 inflammatory metabolite produced by immune cells (Rosani et al., 2019), as a function of
370 bathymetry. We showed that the itaconate relative amount increased in oysters at Low and
371 Middle bathymetry (**Fig. 5**), which presented a high virus load. In contrast, oysters at High
372 bathymetry, with a low virus load, presented an itaconate amount decreased by 10 times (**Fig.**
373 **5**).

374 **Figure 5. Metabolic analysis of Itaconate relative amount.** Relative quantification of the
375 metabolite itaconate in oysters (n=3 per level) at Low (1,6 m), Middle (3 m), and High (5 m)
376 bathymetry. Data are calculated as the area under the curve and expressed in arbitrary units as
377 mean ± SE (*$p<0.05$).

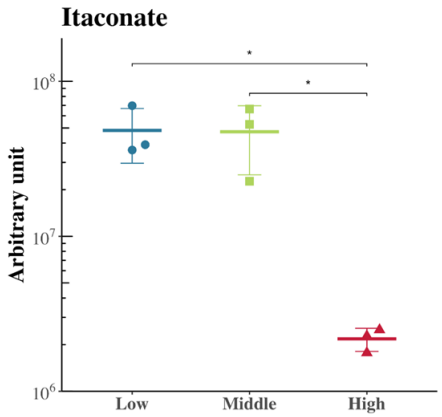

378

379

380 3.6 **Proteomic changes in intertidal oysters**

381 Proteomic analyses identified 55 proteins differentially expressed in oysters as a function of the
382 Middle and High bathymetry compared to Low bathymetry ($p \leq 0.05$; **Fig. 6**). **Table 4** shows
383 the list of identified proteins and the functional properties associated, based on the Uniprot
384 database (http://www.uniprot.org/). The proteins differentially expressed were mitochondrial,
385 transmembrane, and cytoplasmic, among them, 10 proteins still had an unknown function.

386 **Figure 6. Proteomic analysis.** Heatmap representing significantly differentially expressed
387 proteins (55 in total) in the mitochondrial-enriched protein fraction of oysters (pools of n= 10
388 individuals) at Low (1,6 m), Middle (3 m), and High (5 m) bathymetry. Enrichment intensity is
389 expressed as the ratio between proteins up-regulated (red heat) and down-regulated (green heat)
390 normalized with the total.

391

Journal Pre-proof

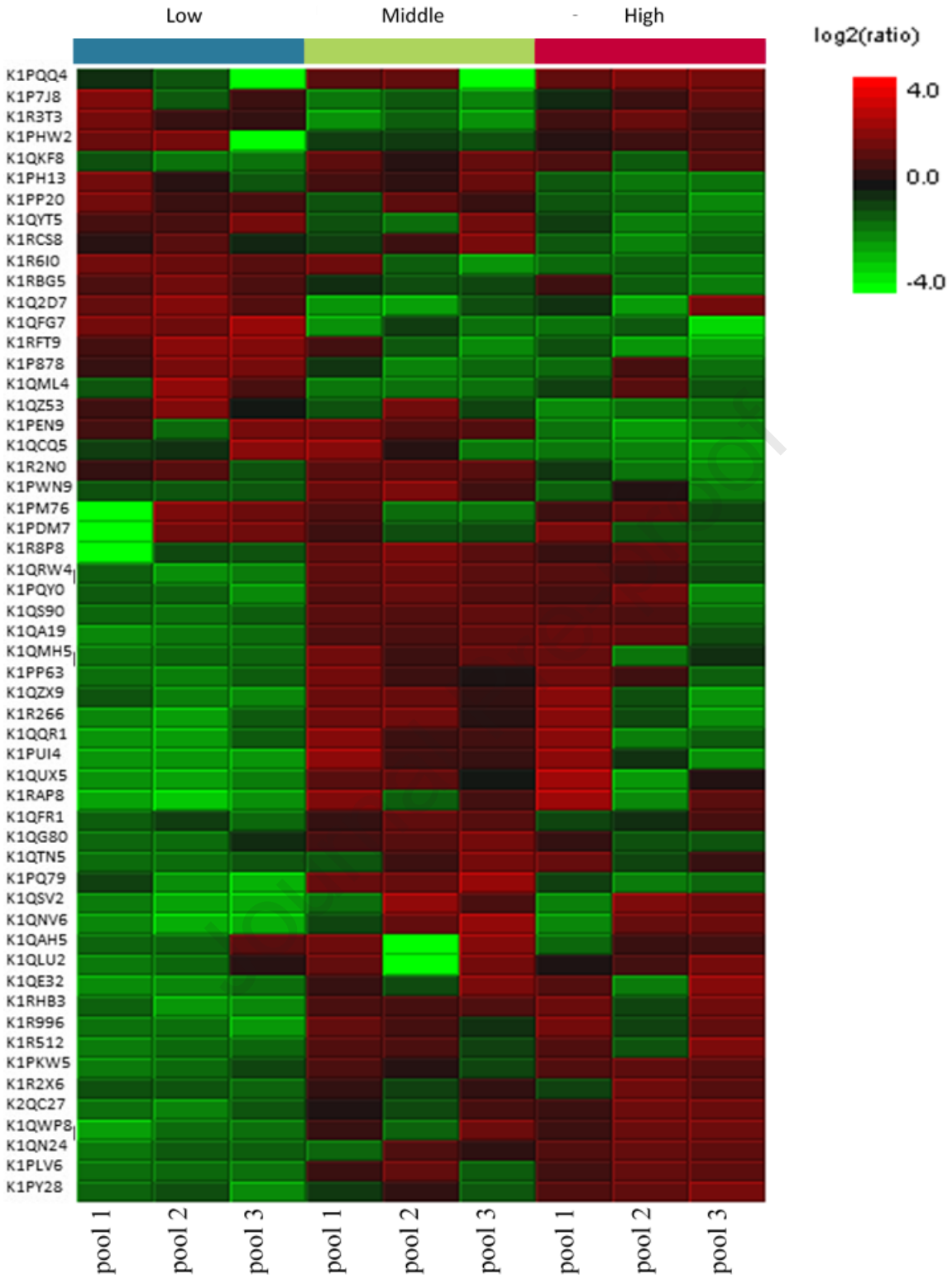
Low
Middle
High
log2(ratio)
4.0
0.0
-4.0
K1PQQ4
K1P7J8
K1R3T3
K1PHW2
K1QKF8
K1PH13
K1PP20
K1QYT5
K1RCS8
K1R6I0
K1RBG5
K1Q2D7
K1QFG7
K1RFT9
K1P878
K1QML4
K1QZ53
K1PEN9
K1QCQ5
K1R2N0
K1PWN9
K1PM76
K1PDM7
K1R8P8
K1QRW4
K1PQY0
K1QS90
K1QA19
K1QMH5
K1PP63
K1QZX9
K1R266
K1QQR1
K1PUI4
K1QUX5
K1RAP8
K1QFR1
K1QG80
K1QTN5
K1PQ79
K1QSV2
K1QNV6
K1QAH5
K1QLU2
K1QE32
K1RHB3
K1R996
K1R512
K1PKW5
K1R2X6
K2QC27
K1QWP8
K1QN24
K1PLV6
K1PY28
pool 1
pool 2
pool 3
pool 1
pool 2
pool 3
pool 1
pool 2
pool 3

392

393

394

395 **Table 4.** Identification of proteins down-expressed (bold in grey) or over-expressed at Middle
396 and High compared to Low bathymetry (significance ≥ 10 using ANOVA). The abundance of
397 proteins was expressed as a ratio by comparison with Low (ratio = 1).

Uniprot accession	NCBI accession	Protein name	Significance	Ratio			Biological process
				Low	Middle	High	
K1PQQ4	CGI 10008275	L-rhamnonate dehydratase	11.34	1	1.48	1.72	Carbohydrate metabolism
K1P7J8	CGI 10008151	6-phosphofructokinase	11.86	1	0.53	0.94	Glycolysis
K1R3T3	CGI 10019268	Transcription factor BTF3	13.48	1	0.45	0.98	Transcription
K1PHW2	CGI 10012107	*Unknown*	18.49	1	0.59	0.72	Membrane cell adhesion
K1QKF8	CGI 10022811	S-(hydroxymethyl)glutathione dehydrogenase	14.01	1	1.75	1.50	Detoxification
K1PH13	CGI 10012206	Glycosyltransferase subunit STT3B	14.21	1	1.06	0.61	Protein N-glycosylation
K1PP20	CGI 10013293	Ependymin-related protein 1	10.51	1	0.85	0.56	Cell matrix adhesion
K1QYT5	CGI 10012871	Phosphate carrier protein	10.08	1	0.79	0.55	OXPHOS Mitochondrial carrier
K1RCS8	CGI 10013133	Metalloendopeptidase	10.12	1	1.11	0.64	Mitochondria quality control
K1R610	CGI 10017526	*Unknown*	22.41	1	0.64	0.49	*Unknown*
K1RBG5	CGI 10021542	4-hydroxybutyrate coenzyme A transferase	10.57	1	0.70	0.63	Detoxification
K1Q2D7	CGI 10004665	Putative ubiquitin carboxyl-terminal hydrolase FAF-X	10.92	1	0.37	0.66	Protein deubiquitination
K1QFG7	CGI 10005276	Galactocerebrosidase	13.48	1	0.46	0.37	Glycolipids catabolism
K1RFT9	CGI 10023709	L-rhamnose-binding lectin	12.56	1	0.49	0.34	Innate immunity
K1P878	CGI 10007259	Universal stress protein	10.8	1	0.51	0.57	Resistance to stress
K1QML4	CGI 10018739	*Unknown*	10.48	1	0.46	0.72	AA catabolism
K1QZ53	CGI 10013854	*Unknown*	12.11	1	0.84	0.47	*Unknown*
K1PEN9	CGI 10001281	Endoglucanase	16.76	1	1.14	0.48	Carbohydrate metabolism
K1QCQ5	CGI 10016417	Succinate-CoA ligase subunit β	10.12	1	0.92	0.41	KREBS cycle
K1R2N0	CGI 10008056	Histone H4	10.12	1	1.22	0.67	Transcription initiation
K1PWN9	CGI_10010245	Mannose receptor 1	10.42	1	1.71	0.96	Membrane receptor (pathogen)
K1PM76	CGI_10020978	NADH dehydrogenase 1α subunit 9	11.73	1	0.52	0.68	OXPHOS complex I
K1PDM7	CGI_10008106	Multidrug resistance-associated protein 1	14.96	1	0.62	0.70	Resistance to stress
K1R8P8	CGI_10024629	Neprilysin	16.18	1	1.65	1.23	Inflammation
K1QRW4	CGI_10025126	Coronin	15.92	1	2.2	1.59	Cytoskeleton dynamic
K1PQY0	CGI_10010860	*Unknown*	12.07	1	1.90	1.56	*Unknown*
K1QS90	CGI_10002881	Neuroglian	25.26	1	1.79	1.45	Cell adhesion
K1QA19	CGI_10015782	Calmodulin-like protein 3	19.18	1	2.01	1.98	Resistance to stress
K1QMH5	CGI_10018703	Small nuclear ribonucleoprotein Sm D1	14.98	1	1.88	1.42	Splicing
K1PP63	CGI_10005728	Carboxylic ester hydrolase	11.89	1	1.83	1.67	Detoxification
K1QZX9	CGI_10014226	*Unknown*	12.81	1	2.01	1.74	*Unknown*
K1R266	CGI_10026868	Retinal dehydrogenase 1	11.06	1	2.38	1.93	Detoxification
K1QQR1	CGI_10024475	Major vault protein	10.46	1	2.58	2.00	Innate immunity
K1PUI4	CGI_10005346	Peptidylprolyl isomerase	13.38	1	3.27	3.04	Chaperone
K1QUX5	CGI_10021866	Omega-crystallin	17.85	1	2.55	2.91	Detoxification
K1RAP8	CGI_10002873	Malic enzyme	11.87	1	3.30	3.88	Lipid metabolism

K1QFR1	CGI_10013834	Beta-1,3-glucan-binding protein	13	1	1.53	1.26	Innate immunity
K1QG80	CGI_10018743	*Unknown*	11.36	1	1.66	1.14	*Unknown*
K1QTN5	CGI_10010936	Collagen alpha-1(XIV) chain	10	1	1.69	1.38	Cell adhesion
K1PQ79	CGI_10011897	Copine-3 ser thr kinase	13.4	1	3.08	1.33	Cell adhesion
K1QVS2	CGI_10009327	Thioredoxin domain-containing protein 5	10.2	1	3.17	2.91	Chaperone
K1QNV6	CGI_10013164	Tropomyosin	13.97	1	3.98	2.99	Cytoskeleton dynamic
K1QAH5	CGI_10012180	Integrin beta	10.57	1	1.86	1.06	Cell adhesion
K1QLU2	CGI_10017638	Serine protease inhibitor dipetalogastin	11.12	1	1.90	1.61	Inflammation
K1QE32	CGI_10018790	Acyl-CoA dehydrogenase	10.67	1	2.16	2.23	Lipid metabolism
K1RHB3	CGI_10022015	Phosphoenolpyruvate phosphomutase	11.61	1	2.08	2.32	Reservoir of organic phosphorus
K1R996	CGI_10001478	Long-chain-fatty-acid-CoA ligase 4	13.47	1	2.01	2.24	Lipid metabolism
K1R512	CGI_10026535	*Unknown*	14.63	1	1.53	1.75	*Unknown*
K1PKW5	CGI_10008456	*Unknown*	13.66	1	1.41	1.72	*Unknown*
K1R2X6	CGI_10018375	*Unknown*	12.75	1	1.26	1.53	*Unknown*
K1QC27	CGI_10023479	Hydroxysteroid dehydrogenase-like protein 2	14.12	1	1.49	1.98	Lipid metabolism
K1QWP8	CGI_10022729	Actin-2	11.99	1	1.89	2.32	Cytoskeleton dynamic
K1QN24	CGI_10017980	Carboxypeptidase B	18.5	1	1.36	1.81	Proteolysis
K1PLV6	CGI_10007483	F-actin-capping protein subunit alpha	20.75	1	1.58	1.87	Cytoskeleton dynamic
K1PY28	CGI_10006807	Sarcoplasmic calcium-binding protein	13.62	1	1.35	2.01	Cytoskeleton dynamic

3.6.1 Metabolic reprogramming in intertidal oysters.

The expression of 16 metabolic proteins was modified in intertidal oysters at Middle and High bathymetry (27% of proteomic changes), indicating a metabolic reprogramming in oysters supporting the fluctuating environment despite we were not able to detect any modifications in total energy reserves in the whole body (Appendix Table A.1). The L-rhamnonate dehydratase (K1PQQ4), implicated in fructose and mannose metabolism, was up-regulated and the 6-phosphofructokinase (K1P7J8) which catalyzes the phosphorylation of fructose-6-phosphate to fructose 1,6-bisphosphate during glycolysis, was down-regulated. Protein N-glycosylation (K1PH13) and protein deubiquitination (K1Q2D7) were down-regulated and carbohydrate metabolism was also decreased (glycolipids K1QFG7 and cellulose catabolism K1PEN9). As further evidence of metabolic changes, the detoxification of phase 1 metabolic products was enhanced (detoxification of ethanol: K1QKF8; xenobiotic: K1PP63; aldehyde: K1R266, K1QUX5; other: K1RBG5). Proteomic changes also concerned the regulation of lipid metabolism suggesting an acceleration of the lipid's turn-over (synthesis and oxidation). Indeed, both the malic enzyme (K1RAP8), which conducts excess ethanol-derived energy into lipid synthesis, and the mitochondrial long-chain specific Acyl-CoA dehydrogenase (K1QE32),

that catalyzes the first step of the fatty-acid beta-oxidation, were up-regulated, as well as the Long-chain-FA-CoA ligase 4 (K1R996) that catalyzes the conversion of long-chain FA to their active form acyl-CoA before lipogenesis and lipolysis. The up-regulation of the hydroxysteroid dehydrogenase (K1QC27) reflected changes in steroid metabolism and an increased amount of carboxypeptidase B was indicative of changes in the digestive gut of intertidal oysters (Yang et al., 2020).

3.6.2 Changes in mitochondrial metabolism in intertidal oysters.

Changes in mitochondrial metabolism were reflected by the differential expression of 4 mitochondrial proteins (6% of proteomic changes). The phosphate carrier protein (K1QYT5) which is located in the mitochondrial inner membrane and catalyzes the transport of phosphate ions for oxidative phosphorylation OXPHOS, and the NADH dehydrogenase 1α subunit 9 (K1PM76) which is involved in the mitochondrial respiratory chain (OXPHOS complex I), were down-regulated. Expression of the mitochondrial metalloendopeptidase (K1RCS8), involved in the quality control system of the inner membrane of mitochondria under stress, was decreased in intertidal oysters at High bathymetry. The Succinate-CoA ligase subunit β (K1QCQ5), a matrix mitochondrial protein that hydrolyses succinyl-CoA for the synthesis of ATP, was down-regulated, indicating a lower mitochondrial TCA functioning (KREBS cycle).

3.6.3 Boost of inflammation and immunity in intertidal oysters.

Differential expression of 19 proteins (32% of proteomic changes) concerned inflammation and immunity. Lectins are critical immune effectors of cellular defense in hemocytes of marine invertebrates (He et al., 2015; Watanabe et al., 2009) and we showed that two transmembrane lectin receptors (K1RFT9, K1PWN9) were down-regulated. The changes observed in the expression of the mannose receptor 1 (K1PWN9), a membrane receptor of immune cells involved in pathogen recognition (Jia et al., 2021), were indicative of changes in immunity. Neprilysin (K1R8P8), an invertebrate immunoregulator, was up-regulated and it is a membrane biomarker of activated hemocytes (Ottaviani et al., 2012). Up-regulation of major vault protein (K1QQR1) and beta-1,3-glucan-binding protein (K1QFR1) reflected increased responsiveness of the innate immune system to the internalization of pathogens (Jenkins, 2008; Melillo et al., 2018; Phupet et al., 2018). The immune Ser-protease inhibitor (K1QLU2) was up-regulated, reflecting enhanced protection against pathogens or parasites (Kanost, 1999). Associated with the boost in immunity, our results showed an increase in cytoskeletal and cell dynamics reflected by the up-regulation of 9 proteins (cell-matrix adhesion K1PP20; coronin K1QRW4; neuroglian K1QS90; collagen alpha-1 chain K1QTN5; copine 3 ser-thr kinase K1PQ79; tropomyosin K1QNV6; integrin beta K1QAH5; actin-2 K1QWP8; F-actin-capping protein

subunit alpha K1PLV6; sarcoplasmic calcium-binding protein K1PY28), as well as the increase of chaperone activity (Chawsheen et al., 2018) (Peptidylpropyl isomerase K1PU14; thioredoxin domain-containing protein 5 K1QVS2) reflecting changes in vesicular transport, cell migration and cell structure in intertidal oysters. All of these processes are involved in the immune reactions of hemocytes (Rybakin and Clemen, 2005).

3.6.4 Stress proteins in intertidal oysters.

Differential expression of 6 stress proteins (10% of proteomic changes) was evidenced. The universal stress protein USP (K1P878) and the Multidrug resistance-associated protein 1, an ATP-binding mitochondrial transmembrane transporter (K1PDM7), were down-regulated in intertidal oysters submitted to environmental fluctuations, although both proteins are expressed under environmental multi-stress in animals, plants and bacteria (Tkaczuk et al., 2013; Vollmer and Bark, 2018). Calmodulin-like protein 3 (K1QA19), a stress-signal transductor involved in Ca^{2+} signaling pathways activated by environmental stress or pathogens, was up-regulated. In addition, the down-regulation of the transcription factor BTF3 from the ARN polymerase II complex (K1R3T3) and up-regulation of the splicing factor ribonucleoprotein SmD1 (K1QMH5) and histone H4 (K1R2N0) indicated important changes in the regulation of gene expression in intertidal oysters.

3.6.5 Intertidal oysters at the upper natural limit of bathymetry.

Interestingly, intertidal oysters reared at the upper limit of bathymetry (High) specifically down-regulated 5 proteins as compared to intertidal oysters at Middle bathymetry. Down-regulation of the mannose receptor 1 (K1PWN9) was indicative of lowered immune cells' pathogen recognition (Jia et al., 2021). The mitochondrial metalloendopeptidase (K1RCS8), which stimulates the mitochondrial quality control mechanisms in response to hypoxia-reoxygenation stress in *C. gigas* (Sokolov et al., 2019), was down-regulated, reflecting that the mitochondrial functioning might be more deeply modified at High bathymetry. The subunit STT3B (K1PH13) was lowered, indicating fewer misfolded proteins in the endoplasmic reticulum, *i.e.* no ER stress for intertidal oysters at High bathymetry despite their harsh conditions. Down-regulated endoglucanase (K1PEN9) reflected lowered cellulose catabolic process and down-regulation of histone H4 (K1R2N0), a core component of the nucleosome (Keating and El-Osta, 2015; Zacchi et al., 2010), might reflect some chromosome decondensation at High bathymetry.

4. **DISCUSSION**

4.1 **Host-pathogen interaction is modulated by the bathymetry.**

C. gigas are exposed to a gradient of environmental stress along subtidal and intertidal habitats that shapes their phenotype, such as increased tolerance to hypoxia in intertidal oysters (Meng et al., 2018). Here we showed that intertidal oysters reared at 3.5 and 6 meters of bathymetry delayed by ten days the onset of the mortality induced by OsHV-1 and increased their final survival by a maximum of 17%. Previous field experiments showed that the final survival rate increased by 8% (Pernet et al., 2019) or 15% (Azéma et al., 2017) in intertidal oysters. Here we showed that intertidal oysters did not modify their energetic composition (carbohydrates, TAG/sterol, total protein amount), but revealed some proteomic changes indicative of metabolic reprogramming in response to harsh environmental conditions. Intertidal oysters at Middle bathymetry remained susceptible to OsHV-1 infection, indicating that the metabolic reprogramming and the reduced immersion time, generating less contact time with the virus in seawater, did not block the viral infection. As a response to the viral attack, oysters at Low and Middle bathymetry over-expressed key immune-responsive genes (*Cg-IAP, Cg-IκB2,* and *Cg-PKR)* and increased production of the metabolite itaconate, independently of their habitat. Itaconate was already characterized as a non-specific immunological biomarker of pathogens in marine bivalves, such as *C. gigas* oyster larvae infected by OsHV-1 and *Pena canaliculus* mussels infected by *vibrio splendidus* (Nguyen et al., 2019, 2018; Van Nguyen and Alfaro, 2019). These changes in gene expression combined with itaconate production reflected a strong anti-viral immune response that was similar in subtidal or intertidal oysters that presented a high virus load, despite their differences in environmental conditions. However, such anti-viral response did not predict the oyster susceptibility to death since oysters at Middle remained better protected from mortality. All together, our results indicated that a harsh intertidal environment can influence gene expression and metabolite production in *C. gigas* without altering their ability to activate an anti-viral immune response.

4.2 **Immune-metabolism is modified by bathymetry.**

No deep changes in energetic reserves were obtained at the level of the whole body, consistent with the similar carbohydrates, lipid, and protein amounts detected. In contrast, the proteomic study highlighted an intertidal metabolic footprint that may confer an advantage to intertidal oysters facing POMS, through an interaction between environment, metabolism, and immunity, also called immune-metabolism (Galenza and Foley, 2019). The intertidal oysters at Middle and High bathymetry reprogrammed their metabolism toward enhanced neoglucogenesis, increased lipid turn-over, and decreased OXPHOS, with activation of inflammation and innate immunity. These proteomic changes delayed the onset of first mortalities but did not block OsHV-1 intracellular processes, since intertidal oysters at Middle bathymetry were infected by

OsHV-1. Thanks to our study, we can emphasize that intertidal oysters delayed the mortality because they might be better protected against bacteria, the second step of POMS, rather than against the virus, the first step of POMS. Indeed, before our experiment, we deployed 1-year-old *C. gigas* spat in the field to study the bathymetric influence on their microbiota (Offret et al., 2020). We proved that the diversity of endogenous microbiota in the digestive gland of oysters was shaped by intertidal conditions at Middle and High bathymetry *(Offret et al., 2020).* In our study, we can suppose that intertidal oysters at Middle and High bathymetry have modified their interaction with bacteria, among them the opportunistic bacteria involved in the polymicrobial disease (de Lorgeril et al., 2018). Interestingly, among proteomic changes in intertidal oysters, we detected an increased amount of carboxypeptidase B (Yang et al., 2020) suggesting that their digestive gut system might have been modified. As demonstrated in fish, the gut system is considered an important component of adaptive immunity and resistance to viral disease (Talwar et al., 2018). As compared to subtidal oysters, intertidal oysters could thus have shaped their digestive bacterial microbiota as a result of harsh environmental conditions (Offret et al., 2020), leading to better protection against fatal bacteremia during POMS (de Lorgeril et al., 2018). Unfortunately, we were not able to analyze bacterial load and diversity in infected oysters in our study. Studying the effects of bathymetry on oyster microbiota during POMS is now of further interest.

4.3 **Mitochondria is involved in host-pathogen interactions.**

Oysters at Low and Middle bathymetry presented a high amount of OsHV-1 DNA, activated an immune antiviral response, increased lysosomal activity, and increased itaconate production. Itaconate is an anti-inflammatory metabolite that is produced by immune cells in *C.gigas*, as shown in response to an exacerbated inflammatory response during OsHV-1 or bacterial infection (Nguyen et al., 2019; Van Nguyen and Alfaro, 2019; Young et al., 2017). Thus, itaconate might play a role in OsHV-1 intracellular processes during POMS by targeting the mitochondria. In vertebrates, itaconate regulates innate immunity and inflammation by targeting the mitochondrial metabolism, by blocking the mitochondrial succinate dehydrogenase (Domínguez-Andrés et al., 2019; Hooftman and O'Neill, 2019; Liao et al., 2019; Mills et al., 2018; O'Neill and Artyomov, 2019). It participates in the type I interferon pathway, a key element of immune cell activation. Under pathogen infection, itaconate can lead to fatal immune paralysis, as a poison of the mitochondria (O'Neill et al., 2016). Itaconate could serve the virus to manipulate the mitochondria to its advantage, such as many viruses in vertebrates and invertebrates controlling host cell machineries by inhibition of specific signaling pathways (Chen et al., 2011; Rosani et al., 2019; Sanchez and Lagunoff, 2015; Su et

al., 2014; Young et al., 2017), these pathways being conserved in *C. gigas* (Epelboin et al., 2016). Itaconate is a key component of metabolic reprogramming in immune cells in vertebrates, linking cell metabolism and the Warburg effect with oxidative and immune responses (Domínguez-Andrés et al., 2019; Hooftman and O'Neill, 2019; O'Neill and Artyomov, 2019). Further studies should be conducted to study the effect of itaconate on the mitochondrial functioning and cell metabolism in *C. gigas*, in particular its role in the Warburg effect that plays in favor of OsHV-1 (Corporeau et al., 2014).

4.4 **Can bathymetry cause environmental fever?**

In the field, oysters are permissive to OsHV-1 when immersed in seawater between 16°C to 24°C (Pernet et al., 2012). In experimental conditions, immersion in seawater at 29°C induces profound transcriptomic changes that promote oyster survival to OsHV-1, by up-regulation of immune regulatory, anti-apoptosis, and protein process genes, and down-regulation of catabolism, metabolite transport, and growth genes, reflecting changes in the metabolism under thermal stress that decrease their susceptibility (Delisle et al., 2020, 2018). In our study, we observed that intertidal oysters delayed mortality when they spent several hours above 24°C and 29°C in air temperature. A heat-stress response might have been activated in oysters at Middle and High bathymetry, as detected in our proteomic analyses through the over-expression of two chaperone molecules involved in protein folding (Peptidylprolyl isomerase, Thioredoxin domain-containing protein 5). As ectotherms, *C. gigas* physiology and response to pathogens are controlled by temperature and intertidal oysters could thus benefit from an "environmental fever" during emersion. It could resemble the "behavioral fever" of ectothermic vertebrates, such as zebrafish moving to warmer environments to amplify their innate immunity against viral disease (Boltaña et al., 2013; Jia et al., 2014). Indeed, in plants and invertebrates, the innate immune system is shaped by the environment and lifestyle (diet and microenvironment) (Melillo et al., 2018), the heat-stress amplifying immune training, as demonstrated in shrimp (Jia et al., 2014). Such immune training can even confer an immunological memory, also called immune priming, resulting in a faster and more effective response to stress (Melillo et al., 2018; Netea et al., 2020). We already know that immune priming is possible in *C. gigas* after poly I:C injection that induced an antiviral alert and protected oysters from POMS for 4 months (Lafont et al., 2020). Thus, the intertidal environment could have activated a sort of "environmental priming" of *C. gigas*, involving a thermal stress-response mimicking the "behavioral fever" of mobile species such as fish. Further experiments are needed to decipher whether immune cells of intertidal oysters were

583 primed transiently or long-term, and if they modified their epigenetic status, as a signal of
584 "environmental priming".

585 5. **CONCLUSION**

586 Our work demonstrated that fluctuating environmental dynamics influence the plasticity of
587 metabolism and immunity in *C. gigas*. The intertidal environment can boost metabolic,
588 inflammation, and immune state in juvenile *C. gigas* in a way that modifies interaction with
589 pathogens and promotes resistance to POMS. We propose to take advantage of the important
590 metabolic plasticity of the Pacific oyster *C. gigas* to adapt to challenging coastal environments
591 as a model species to study cellular responses to a harsh environment and the impact of global
592 changes on animal health.

593 6. **APPENDIX**

594 **Table A.1: Biochemical analyses of carbohydrates, lipids, and total protein amounts.** Five
595 samples of powder (250 mg each) were pooled for biochemical analyses (1 pool of 5 individuals
596 per bag). Analyses were done in technical triplicates and data are means ± SE (n= 1 pool x 3
597 bags x 3 bathymetric levels). 50 mg of nitrogen powder was homogenized in 2 ml of nanopure
598 water using a Polytron® PT 2500 E (Kinemetica, Luzernerstrasse, Switzerland), diluted 10
599 times and carbohydrate concentration was determined by a colorimetric method (DuBois et al.,
600 1956) using a standard calibration curve. Neutral and polar lipids class were determined with a
601 CAMAG automatic sampler (CAMAG, Moirans, France) after extraction with 200 mg of
602 powder added to 4 ml chloroform-methanol (2:1, v/v; Folch et al., 1957). Total protein
603 extraction was done on 450 mg of powder homogenized with a Polytron® PT 2500 E
604 (Kinemetica, Malters, Switzerland) in 5 mL of lysis buffer (Guévélou et al., 2013). Total protein
605 content in each lysate was analyzed using the DC protein assay (Bio-Rad) in 96-well
606 microplates (Nunc™) using a microplate reader (Bio-Tek®SynergyTM HT, Thermo Fisher
607 Scientific, Les Ulis, France). Total protein concentration was obtained using Gen5 version 2.03
608 software (Bio-Tek).

	Carbohydrates (µg/mg flesh)	Triacylglycerol/sterol (arbitrary unit)	Protein (µg/ml flesh)
High (5 m)	55,16 ± 7,11	4,43 ± 0,41	51,99 ± 7,51
Middle (3 m)	51,32 ± 3,14	5,76 ± 0,48	51,41 ± 1,58
Low (1.6 m)	60,66 ± 17,77	5,83 ± 1,18	40,99 ± 11,59

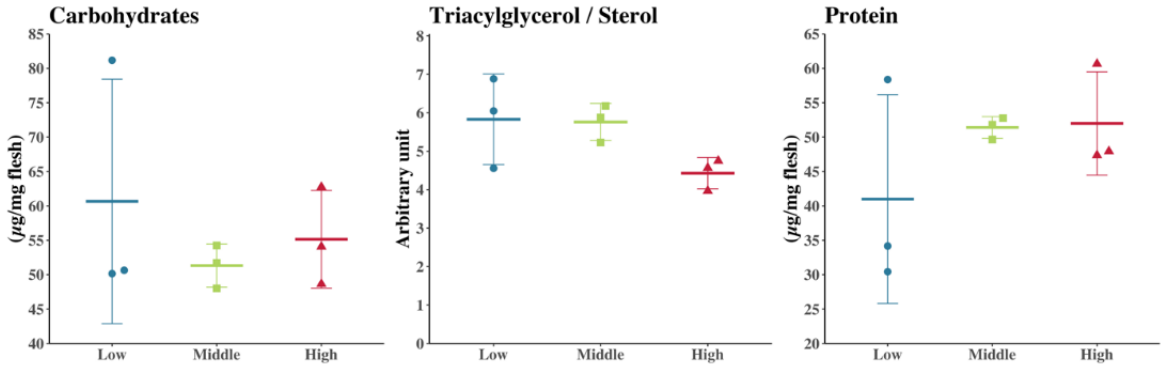

AUTHOR CONTRIBUTIONS

C. Corporeau: Conceptualization, Funding acquisition, Investigation, Methodology, Project administration, Supervision, Validation, Roles/Writing-original draft, Writing-review and editing; **S. Petton:** Data curation, Visualization; **R. Vilaça:** Formal analysis, Roles/Writing-original draft; **L. Delisle:** Formal analysis, Investigation, Methodology, Roles/Writing-review and editing; **C. Quéré:** Investigation, Methodology. **V. Le Roy:** Investigation; **C. Dubreuil:** Investigation; **S. Lacas-Gervais:** Investigation, Methodology; **Y. Guitton:** Formal analysis, Investigation, Methodology; **S. Artigaud:** Formal analysis, Investigation, Validation; **B. Bernay:** Data curation, Formal analysis, Investigation, Methodology; **V. Pichereau;** Funding acquisition, Roles/Writing-review and editing; **A. Huvet:** Formal analysis, Roles/Writing-original draft, Writing-review and editing; **B. Petton:** Conceptualization, Methodology, Roles/Writing-original draft; **F. Pernet:** Formal analysis, Validation; **E. Fleury:** Formal analysis, Roles/Writing-review and editing; **S. Madec:** Roles/ Writing-review and editing; **C. Brigaudeau:** Conceptualization, Investigation, Roles/Writing-review and editing; **C. Brenner:** Conceptualization, Funding acquisition, Supervision, Validation, Roles/Writing-original draft; **N. Mazure:** Conceptualization, Funding acquisition, Supervision, Validation, Roles/Writing-original draft.

ACKNOWLEDGMENTS

This work was supported by Labex Mer (BODY project), the “Fondation ARC pour la recherche sur le cancer” (MOLLUSC project), and the ECOSCOPA network founded by the French Ministry of the DPMA. We acknowledge the Ifremer staff at Ifremer Argenton and Bouin and Fanny Langlois for technical help in biochemistry, University’s CCMA Electron Microscopy facility (supported by Université de Nice Sophia-Antipolis, Region Sud Est Provence Alpes-Cote d’Azur, Conseil Départemental 06, and Gis Ibisa) and Alyssia Marie for technical help in microscopy. We thank the Biogenouest-Corsaire core facility for metabolome

636 analyses done with the instrumental facilities LABERCA. We thank Morgan Smits from Lemar
637 for the English revision of the text.

638 7. **REFERENCES**

639 Alfaro, A.C., Young, T., 2018. Showcasing metabolomic applications in aquaculture: a review. Reviews
640 in Aquaculture 10, 135–152. https://doi.org/10.1111/raq.12152
641 Azéma, P., Maurouard, E., Lamy, J.-B., Dégremont, L., 2017. The use of size and growing height to
642 improve Crassostrea gigas farming and breeding techniques against OsHV-1. Aquaculture
643 471, 121–129. https://doi.org/10.1016/j.aquaculture.2017.01.011
644 Bayne, B.L., 2017. Metabolic Expenditure, in: Developments in Aquaculture and Fisheries Science.
645 Elsevier, pp. 331–415. https://doi.org/10.1016/B978-0-12-803472-9.00006-6
646 Boltaña, S., Rey, S., Roher, N., Vargas, R., Huerta, M., Huntingford, F.A., Goetz, F.W., Moore, J.,
647 Garcia-Valtanen, P., Estepa, A., MacKenzie, S., 2013. Behavioural fever is a synergic signal
648 amplifying the innate immune response. Proc Biol Sci 280.
649 https://doi.org/10.1098/rspb.2013.1381
650 Cesbron, N., Royer, A.-L., Guitton, Y., Sydor, A., Le Bizec, B., Dervilly-Pinel, G., 2017. Optimization of
651 fecal sample preparation for untargeted LC-HRMS based metabolomics. Metabolomics 13,
652 99. https://doi.org/10.1007/s11306-017-1233-8
653 Chawsheen, H.A., Ying, Q., Jiang, H., Wei, Q., 2018. A critical role of the thioredoxin domain
654 containing protein 5 (TXNDC5) in redox homeostasis and cancer development. Genes &
655 Diseases 5, 312–322. https://doi.org/10.1016/j.gendis.2018.09.003
656 Chen, I.-T., Aoki, T., Huang, Y.-T., Hirono, I., Chen, T.-C., Huang, J.-Y., Chang, G.-D., Lo, C.-F., Wang, H.-
657 C., 2011. White Spot Syndrome Virus Induces Metabolic Changes Resembling the Warburg
658 Effect in Shrimp Hemocytes in the Early Stage of Infection. J. Virol. 85, 12919–12928.
659 https://doi.org/10.1128/JVI.05385-11
660 Corporeau, C., Huvet, A., Pichereau, V., Delisle, L., Quéré, C., Dubreuil, C., Artigaud, S., Brenner, C.,
661 Meyenberg Cunha-De Padua, M., Mazure, N., 2019. *Crassostrea gigas* , une huître au service
662 de la recherche sur le cancer. médecine/sciences 35, 463–466.
663 https://doi.org/10.1051/medsci/2019079
664 Corporeau, C., Tamayo, D., Pernet, F., Quéré, C., Madec, S., 2014. Proteomic signatures of the oyster
665 metabolic response to herpesvirus OsHV-1 µVar infection. J Proteomics 109, 176–187.
666 https://doi.org/10.1016/j.jprot.2014.06.030
667 de Lorgeril, J., Lucasson, A., Petton, B., Toulza, E., Montagnani, C., Clerissi, C., Vidal-Dupiol, J.,
668 Chaparro, C., Galinier, R., Escoubas, J.-M., Haffner, P., Dégremont, L., Charrière, G.M., Lafont,
669 M., Delort, A., Vergnes, A., Chiarello, M., Faury, N., Rubio, T., Leroy, M.A., Pérignon, A.,
670 Régler, D., Morga, B., Alunno-Bruscia, M., Boudry, P., Le Roux, F., Destoumieux-Garzón, D.,
671 Gueguen, Y., Mitta, G., 2018. Immune-suppression by OsHV-1 viral infection causes fatal
672 bacteraemia in Pacific oysters. Nat Commun 9, 4215. https://doi.org/10.1038/s41467-018-
673 06659-3
674 Delisle, L., Pauletto, M., Vidal-Dupiol, J., Petton, B., Bargelloni, L., Montagnani, C., Pernet, F.,
675 Corporeau, C., Fleury, E., 2020. High temperature induces transcriptomic changes in
676 *Crassostrea gigas* that hinders progress of Ostreid herpesvirus (OsHV-1) and promotes
677 survival. J Exp Biol jeb.226233. https://doi.org/10.1242/jeb.226233
678 Delisle, L., Petton, B., Burguin, J.F., Morga, B., Corporeau, C., Pernet, F., 2018. Temperature modulate
679 disease susceptibility of the Pacific oyster Crassostrea gigas and virulence of the Ostreid
680 herpesvirus type 1. Fish Shellfish Immunol. 80, 71–79.
681 https://doi.org/10.1016/j.fsi.2018.05.056
682 Domínguez-Andrés, J., Novakovic, B., Li, Y., Scicluna, B.P., Gresnigt, M.S., Arts, R.J.W., Oosting, M.,
683 Moorlag, S.J.C.F.M., Groh, L.A., Zwaag, J., Koch, R.M., Horst, R. ter, Joosten, L.A.B., Wijmenga,
684 C., Michelucci, A., Poll, T. van der, Kox, M., Pickkers, P., Kumar, V., Stunnenberg, H., Netea,
685 M.G., 2019. The Itaconate Pathway Is a Central Regulatory Node Linking Innate Immune

Tolerance and Trained Immunity. Cell Metabolism 29, 211-220.e5. https://doi.org/10.1016/j.cmet.2018.09.003

Donaghy, L., Artigaud, S., Sussarellu, R., Lambert, C., Le Goïc, N., Hégaret, H., Soudant, P., 2013. Tolerance of bivalve mollusc hemocytes to variable oxygen availability: a mitochondrial origin? Aquatic Living Resources 26, 257–261. https://doi.org/10.1051/alr/2013054

DuBois, M., Gilles, K.A., Hamilton, J.K., Rebers, P.A., Smith, F., 1956. Colorimetric Method for Determination of Sugars and Related Substances 2, 7.

Epelboin, Y., Quintric, L., Guévélou, E., Boudry, P., Pichereau, V., Corporeau, C., 2016. The Kinome of Pacific Oyster Crassostrea gigas, Its Expression during Development and in Response to Environmental Factors. PLOS ONE 11, e0155435. https://doi.org/10.1371/journal.pone.0155435

Falfushynska, H., Piontkivska, H., Sokolova, I.M., 2020. Effects of intermittent hypoxia on the cell survival and inflammatory responses in the intertidal marine bivalves Mytilus edulis and Crassostrea gigas. Journal of Experimental Biology. https://doi.org/10.1242/jeb.217026

Fleury, E., Barbier, P., Petton, B., Normand, J., Thomas, Y., Pouvreau, S., Daigle, G., Pernet, F., 2020. Latitudinal drivers of oyster mortality: deciphering host, pathogen and environmental risk factors. Scientific Reports 10, 7264. https://doi.org/10.1038/s41598-020-64086-1

Fleury, E., Normand, J., Lamoureux, A., Bouget, J.-F., Lupo, C., Cochennec-Laureau, N., Petton, S., Petton, B., Pouvreau, S., 2021. RESCO REMORA Database : National monitoring network of mortality and growth rates of the sentinel oyster Crassostrea gigas. https://doi.org/10.17882/53007

Folch, J., Lees, M., Stanley, G.H.S., 1957. A SIMPLE METHOD FOR THE ISOLATION AND PURIFICATION OF TOTAL LIPIDES FROM ANIMAL TISSUES. Journal of Biological Chemistry 226, 497–509. https://doi.org/10.1016/S0021-9258(18)64849-5

Fouad, Y.A., Aanei, C., 2017. Revisiting the hallmarks of cancer. Am J Cancer Res 7, 1016–1036.

Galenza, A., Foley, E., 2019. Immunometabolism: Insights from the Drosophila model. Developmental & Comparative Immunology 94, 22–34. https://doi.org/10.1016/j.dci.2019.01.011

Green, T.J., Robinson, N., Chataway, T., Benkendorff, K., O'Connor, W., Speck, P., 2014. Evidence that the major hemolymph protein of the Pacific oyster, Crassostrea gigas, has antiviral activity against herpesviruses. Antiviral Research 110, 168–174. https://doi.org/10.1016/j.antiviral.2014.08.010

Guévélou, E., Huvet, A., Sussarellu, R., Milan, M., Guo, X., Li, L., Zhang, G., Quillien, V., Daniel, J.-Y., Quéré, C., Boudry, P., Corporeau, C., 2013. Regulation of a truncated isoform of AMP-activated protein kinase α (AMPKα) in response to hypoxia in the muscle of Pacific oyster Crassostrea gigas. J. Comp. Physiol. B, Biochem. Syst. Environ. Physiol. 183, 597–611. https://doi.org/10.1007/s00360-013-0743-6

He, S., Song, L., Qian, Z., Hou, F., Liu, Y., Wang, X., Peng, Z., Sun, C., Liu, X., 2015. Molecular characterization of LvAV in response to white spot syndrome virus infection in the pacific white shrimp (litopenaeus vannamei). Dev. Comp. Immunol. 51, 48–55. https://doi.org/10.1016/j.dci.2015.02.020

Hooftman, A., O'Neill, L.A.J., 2019. The Immunomodulatory Potential of the Metabolite Itaconate. Trends Immunol 40, 687–698. https://doi.org/10.1016/j.it.2019.05.007

Itoh, N., Xue, Q.-G., Schey, K.L., Li, Y., Cooper, R.K., La Peyre, J.F., 2011. Characterization of the major plasma protein of the eastern oyster, Crassostrea virginica, and a proposed role in host defense. Comp. Biochem. Physiol. B-Biochem. Mol. Biol. 158, 9–22. https://doi.org/10.1016/j.cbpb.2010.06.006

Jenkins, D., 2008. Role for Major Vault Protein in the innate immunity of respiratory epithelium. Thorax 63, 107–107.

Jia, X., Wang, F., Lu, Y., Zhang, D., Dong, S., 2014. Immune responses of Litopenaeus vannamei to thermal stress: a comparative study of shrimp in freshwater and seawater conditions. Marine and Freshwater Behaviour and Physiology 47, 79–92. https://doi.org/10.1080/10236244.2014.894349

Jia, Z., Jiang, S., Wang, M., Wang, X., Liu, Y., Lv, Z., Song, X., Li, Y., Wang, L., Song, L., 2021. Identification of a Novel Pattern Recognition Receptor DM9 Domain Containing Protein 4 as a Marker for Pro-Hemocyte of Pacific Oyster Crassostrea gigas. Frontiers in Immunology 11, 3811. https://doi.org/10.3389/fimmu.2020.603270

Kanost, M.R., 1999. Serine proteinase inhibitors in arthropod immunity. Developmental & Comparative Immunology, Invertebrate Immunity 23, 291–301. https://doi.org/10.1016/S0145-305X(99)00012-9

Keating, S.T., El-Osta, A., 2015. Epigenetics and metabolism. Circ. Res. 116, 715–736. https://doi.org/10.1161/CIRCRESAHA.116.303936

Lafont, M., Vergnes, A., Vidal-Dupiol, J., de Lorgeril, J., Gueguen, Y., Haffner, P., Petton, B., Chaparro, C., Barrachina, C., Destoumieux-Garzon, D., Mitta, G., Gourbal, B., Montagnani, C., 2020. A Sustained Immune Response Supports Long-Term Antiviral Immune Priming in the Pacific Oyster, *Crassostrea gigas*. mBio 11, e02777-19, /mbio/11/2/mBio.02777-19.atom. https://doi.org/10.1128/mBio.02777-19

Li, L., Li, A., Song, K., Meng, J., Guo, X., Li, S., Li, C., De Wit, P., Que, H., Wu, F., Wang, W., Qi, H., Xu, F., Cong, R., Huang, B., Li, Y., Wang, T., Tang, X., Liu, S., Li, B., Shi, R., Liu, Y., Bu, C., Zhang, C., He, W., Zhao, S., Li, H., Zhang, S., Zhang, L., Zhang, G., 2018. Divergence and plasticity shape adaptive potential of the Pacific oyster. Nat Ecol Evol 2, 1751–1760. https://doi.org/10.1038/s41559-018-0668-2

Liao, S.-T., Han, C., Xu, D.-Q., Fu, X.-W., Wang, J.-S., Kong, L.-Y., 2019. 4-Octyl itaconate inhibits aerobic glycolysis by targeting GAPDH to exert anti-inflammatory effects. Nature Communications 10, 5091. https://doi.org/10.1038/s41467-019-13078-5

LIN, D.Y., WEI, L.J., YING, Z., 1993. Checking the Cox model with cumulative sums of martingale-based residuals. Biometrika 80, 557–572. https://doi.org/10.1093/biomet/80.3.557

Livak, K.J., Schmittgen, T.D., 2001. Analysis of Relative Gene Expression Data Using Real-Time Quantitative PCR and the 2−ΔΔCT Method. Methods 25, 402–408. https://doi.org/10.1006/meth.2001.1262

Mazaleyrat, A., Normand, J., Dubroca, L., Fleury, E., 2022. A 26-year time series of mortality and growth of the Pacific oyster C. gigas recorded along French coasts. Sci Data 9, 392. https://doi.org/10.1038/s41597-022-01511-2

Melillo, D., Marino, R., Italiani, P., Boraschi, D., 2018. Innate Immune Memory in Invertebrate Metazoans: A Critical Appraisal. Front Immunol 9. https://doi.org/10.3389/fimmu.2018.01915

Meng, J., Wang, T., Li, L., Zhang, G., 2018. Inducible variation in anaerobic energy metabolism reflects hypoxia tolerance across the intertidal and subtidal distribution of the Pacific oyster (Crassostrea gigas). Mar Environ Res 138, 135–143. https://doi.org/10.1016/j.marenvres.2018.04.002

Mills, E.L., Ryan, D.G., Prag, H.A., Dikovskaya, D., Menon, D., Zaslona, Z., Jedrychowski, M.P., Costa, A.S.H., Higgins, M., Hams, E., Szpyt, J., Runtsch, M.C., King, M.S., McGouran, J.F., Fischer, R., Kessler, B.M., McGettrick, A.F., Hughes, M.M., Carroll, R.G., Booty, L.M., Knatko, E.V., Meakin, P.J., Ashford, M.L.J., Modis, L.K., Brunori, G., Sévin, D.C., Fallon, P.G., Caldwell, S.T., Kunji, E.R.S., Chouchani, E.T., Frezza, C., Dinkova-Kostova, A.T., Hartley, R.C., Murphy, M.P., O'Neill, L.A., 2018. Itaconate is an anti-inflammatory metabolite that activates Nrf2 via alkylation of KEAP1. Nature 556, 113–117. https://doi.org/10.1038/nature25986

Morga, B., Faury, N., Guesdon, S., Chollet, B., Renault, T., 2017. Haemocytes from Crassostrea gigas and OsHV-1: A promising in vitro system to study host/virus interactions. Journal of Invertebrate Pathology 150, 45–53. https://doi.org/10.1016/j.jip.2017.09.007

Netea, M.G., Domínguez-Andrés, J., Barreiro, L.B., Chavakis, T., Divangahi, M., Fuchs, E., Joosten, L.A.B., van der Meer, J.W.M., Mhlanga, M.M., Mulder, W.J.M., Riksen, N.P., Schlitzer, A., Schultze, J.L., Stabell Benn, C., Sun, J.C., Xavier, R.J., Latz, E., 2020. Defining trained immunity and its role in health and disease. Nature Reviews Immunology 20, 375–388. https://doi.org/10.1038/s41577-020-0285-6

790 Nguyen, T.V., Alfaro, A.C., Merien, F., Young, T., Grandiosa, R., 2018. Metabolic and immunological
791 responses of male and female new Zealand Greenshell™ mussels (Perna canaliculus) infected
792 with Vibrio sp. Journal of Invertebrate Pathology 157, 80–89.
793 https://doi.org/10.1016/j.jip.2018.08.008
794 Nguyen, T.V., Alfaro, A.C., Young, T., Green, S., Zarate, E., Merien, F., 2019. Itaconic acid inhibits
795 growth of a pathogenic marine Vibrio strain: A metabolomics approach. Scientific Reports 9,
796 5937. https://doi.org/10.1038/s41598-019-42315-6
797 Offret, C., Paulino, S., Gauthier, O., Château, K., Bidault, A., Corporeau, C., Miner, P., Petton, B.,
798 Pernet, F., Fabioux, C., Paillard, C., Blay, G.L., 2020. The marine intertidal zone shapes oyster
799 and clam digestive bacterial microbiota. FEMS Microbiol Ecol 96, 1–12.
800 https://doi.org/10.1093/femsec/fiaa078
801 O'Neill, L.A.J., Artyomov, M.N., 2019. Itaconate: the poster child of metabolic reprogramming in
802 macrophage function. Nature Reviews Immunology 19, 273–281.
803 https://doi.org/10.1038/s41577-019-0128-5
804 O'Neill, L.A.J., Kishton, R.J., Rathmell, J., 2016. A guide to immunometabolism for immunologists. Nat
805 Rev Immunol 16, 553–565. https://doi.org/10.1038/nri.2016.70
806 Ottaviani, E., Malagoli, D., Grimaldi, A., Eguileor, M. de, 2012. The immuneregulator role of neprilysin
807 (NEP) in invertebrates. ISJ-INVERT SURVIV J 9, 207–211.
808 Pauletto, M., Segarra, A., Montagnani, C., Quillien, V., Faury, N., Le Grand, J., Miner, P., Petton, B.,
809 Labreuche, Y., Fleury, E., Fabioux, C., Bargelloni, L., Renault, T., Huvet, A., 2017. Long dsRNAs
810 promote an anti-viral response in Pacific oyster hampering ostreid herpesvirus 1 replication. J
811 Exp Biol 220, 3671–3685. https://doi.org/10.1242/jeb.156299
812 Pepin, J.F., Riou, A., Renault, T., 2008. Rapid and sensitive detection of ostreid herpesvirus 1 in oyster
813 samples by real-time PCR. Journal of Virological Methods 149, 269–276.
814 https://doi.org/10.1016/j.jviromet.2008.01.022
815 Perez-Riverol, Y., Csordas, A., Bai, J., Bernal-Llinares, M., Hewapathirana, S., Kundu, D.J., Inuganti, A.,
816 Griss, J., Mayer, G., Eisenacher, M., Pérez, E., Uszkoreit, J., Pfeuffer, J., Sachsenberg, T.,
817 Yilmaz, S., Tiwary, S., Cox, J., Audain, E., Walzer, M., Jarnuczak, A.F., Ternent, T., Brazma, A.,
818 Vizcaíno, J.A., 2019. The PRIDE database and related tools and resources in 2019: improving
819 support for quantification data. Nucleic Acids Res 47, D442–D450.
820 https://doi.org/10.1093/nar/gky1106
821 Pernet, F., Barret, J., Dégremont, L., Lagarde, F., Pépin, J.-F., Keck, N., 2012. Mass mortalities of
822 Pacific oysters Crassostrea gigas reflect infectious diseases and vary with farming practices in
823 the Mediterranean Thau lagoon, France 23.
824 Pernet, F., Fuhrmann, M., Petton, B., Mazurié, J., Bouget, J.-F., Fleury, E., Daigle, G., Gernez, P., 2018.
825 Determination of risk factors for herpesvirus outbreak in oysters using a broad-scale spatial
826 epidemiology framework. Scientific Reports 8. https://doi.org/10.1038/s41598-018-29238-4
827 Pernet, F., Gachelin, S., Stanisière, J.-Y., Petton, B., Fleury, E., Mazurié, J., 2019. Farmer monitoring
828 reveals the effect of tidal height on mortality risk of oysters during a herpesvirus outbreak.
829 ICES J Mar Sci 76, 1816–1824. https://doi.org/10.1093/icesjms/fsz074
830 Petton, B., Boudry, P., Alunno-Bruscia, M., Pernet, F., 2015. Factors influencing disease-induced
831 mortality of Pacific oysters Crassostrea gigas. Aquaculture Environment Interactions 6, 205–
832 222. https://doi.org/10.3354/aei00125
833 Petton, S., Corporeau, C., Quemener, L., 2020. Temperature monitoring of subtidal and intertidal
834 microhabitats of oyster Crassostrea gigas. SEANOE data set. https://doi.org/10.17882/79095
835 Phupet, B., Pitakpornpreecha, T., Baowubon, N., Runsaeng, P., Utarabhand, P., 2018.
836 Lipopolysaccharide- and β-1,3-glucan-binding protein from Litopenaeus vannamei:
837 Purification, cloning and contribution in shrimp defense immunity via phenoloxidase
838 activation. Developmental & Comparative Immunology 81, 167–179.
839 https://doi.org/10.1016/j.dci.2017.11.016

Rosani, U., Young, T., Bai, C.-M., Alfaro, A.C., Venier, P., 2019. Dual Analysis of Virus-Host Interactions: The Case of *Ostreid herpesvirus* 1 and the Cupped Oyster *Crassostrea gigas*. Evol Bioinform Online 15, 117693431983130. https://doi.org/10.1177/1176934319831305

Rozenn Cannuel, P.G.B., 2005. Is oyster broodstock feeding always necessary? A study using oocyte quality predictors and validators in Crassostrea gigas. Aquat Living Resour 18, 35–43. https://doi.org/10.1051/alr:2005003

Rybakin, V., Clemen, C.S., 2005. Coronin proteins as multifunctional regulators of the cytoskeleton and membrane trafficking. BioEssays 27, 625–632. https://doi.org/10.1002/bies.20235

Sanchez, E.L., Lagunoff, M., 2015. Viral activation of cellular metabolism. Virology, 60th Anniversary Issue 479–480, 609–618. https://doi.org/10.1016/j.virol.2015.02.038

Scanes, E., Parker, L.M., O'Connor, W.A., Stapp, L.S., Ross, P.M., 2017. Intertidal oysters reach their physiological limit in a future high-CO_2 world. J Exp Biol 220, 765–774. https://doi.org/10.1242/jeb.151365

Scotti, P.D., Dearing, S.C., Greenwood, D.R., 2007. Characterisation of cavortin, the major haemolymph protein of the Pacific oyster *(Crassostrea gigas)*. New Zealand Journal of Marine and Freshwater Research 41, 91–101. https://doi.org/10.1080/00288330709509898

Segarra, A., Faury, N., Pépin, J.-F., Renault, T., 2014. Transcriptomic study of 39 ostreid herpesvirus 1 genes during an experimental infection. Journal of Invertebrate Pathology 119, 5–11. https://doi.org/10.1016/j.jip.2014.03.002

Sokolov, E.P., Markert, S., Hinzke, T., Hirschfeld, C., Becher, D., Ponsuksili, S., Sokolova, I.M., 2019. Effects of hypoxia-reoxygenation stress on mitochondrial proteome and bioenergetics of the hypoxia-tolerant marine bivalve Crassostrea gigas. Journal of Proteomics 194, 99–111. https://doi.org/10.1016/j.jprot.2018.12.009

Sokolova, I., 2018. Mitochondrial Adaptations to Variable Environments and Their Role in Animals' Stress Tolerance. Integrative and Comparative Biology 58, 519–531. https://doi.org/10.1093/icb/icy017

Su, M.-A., Huang, Y.-T., Chen, I.-T., Lee, D.-Y., Hsieh, Y.-C., Li, C.-Y., Ng, T.H., Liang, S.-Y., Lin, S.-Y., Huang, S.-W., Chiang, Y.-A., Yu, H.-T., Khoo, K.-H., Chang, G.-D., Lo, C.-F., Wang, H.-C., 2014. An invertebrate Warburg effect: a shrimp virus achieves successful replication by altering the host metabolome via the PI3K-Akt-mTOR pathway. PLoS Pathog. 10, e1004196. https://doi.org/10.1371/journal.ppat.1004196

Sussarellu, R., Dudognon, T., Fabioux, C., Soudant, P., Moraga, D., Kraffe, E., 2013. Rapid mitochondrial adjustments in response to short-term hypoxia and re-oxygenation in the Pacific oyster, Crassostrea gigas. Journal of Experimental Biology 216, 1561–1569. https://doi.org/10.1242/jeb.075879

Sussarellu, R., Fabioux, C., Camacho Sanchez, M., Le Goïc, N., Lambert, C., Soudant, P., Moraga, D., 2012. Molecular and cellular response to short-term oxygen variations in the Pacific oyster Crassostrea gigas. Journal of Experimental Marine Biology and Ecology 412, 87–95. https://doi.org/10.1016/j.jembe.2011.11.007

Sussarellu, R., Suquet, M., Thomas, Y., Lambert, C., Fabioux, C., Pernet, M.E.J., Le Goic, N., Quillien, V., Mingant, C., Epelboin, Y., Corporeau, C., Guyomarch, J., Robbens, J., Paul-Pont, I., Soudant, P., Huvet, A., 2016. Oyster reproduction is affected by exposure to polystyrene microplastics. Proceedings Of The National Academy Of Sciences Of The United States Of America 113, 2430–2435. https://doi.org/10.1073/pnas.1519019113

Talwar, C., Nagar, S., Lal, R., Negi, R.K., 2018. Fish Gut Microbiome: Current Approaches and Future Perspectives. Indian J Microbiol 58, 397–414. https://doi.org/10.1007/s12088-018-0760-y

Tkaczuk, K.L., A Shumilin, I., Chruszcz, M., Evdokimova, E., Savchenko, A., Minor, W., 2013. Structural and functional insight into the universal stress protein family. Evol Appl 6, 434–449. https://doi.org/10.1111/eva.12057

Van Nguyen, T., Alfaro, A.C., 2019. Targeted metabolomics to investigate antimicrobial activity of itaconic acid in marine molluscs. Metabolomics 15, 97. https://doi.org/10.1007/s11306-019-1556-8

Vollmer, A.C., Bark, S.J., 2018. Twenty-Five Years of Investigating the Universal Stress Protein: Function, Structure, and Applications. Adv Appl Microbiol 102, 1–36. https://doi.org/10.1016/bs.aambs.2017.10.001

Wang, Z., Liu, D., Varin, A., Nicolas, V., Courilleau, D., Mateo, P., Caubere, C., Rouet, P., Gomez, A.-M., Vandecasteele, G., Fischmeister, R., Brenner, C., 2016. A cardiac mitochondrial cAMP signaling pathway regulates calcium accumulation, permeability transition and cell death. Cell Death & Disease 7, e2198–e2198. https://doi.org/10.1038/cddis.2016.106

Warburg, O., 1956. On the origin of cancer cells. Science 123, 309–314.

Watanabe, Y., Tateno, H., Nakamura-Tsuruta, S., Kominami, J., Hirabayashi, J., Nakamura, O., Watanabe, T., Kamiya, H., Naganuma, T., Ogawa, T., Naudé, R.J., Muramoto, K., 2009. The function of rhamnose-binding lectin in innate immunity by restricted binding to Gb3. Dev Comp Immunol 33, 187–197. https://doi.org/10.1016/j.dci.2008.08.008

Webb, S.C., Fidler, A., Renault, T., 2007. Primers for PCR-based detection of ostreid herpes virus-1 (OsHV-1): Application in a survey of New Zealand molluscs. Aquaculture 272, 126–139. https://doi.org/10.1016/j.aquaculture.2007.07.224

Whyte, J.N.C., Englar, J.R., Carswell, B.L., 1990. Biochemical composition and energy reserves in Crassostrea gigas exposed to different levels of nutrition. Aquaculture 90, 157–172. https://doi.org/10.1016/0044-8486(90)90338-N

Yang, M.-J., Song, H., Yu, Z.-L., Xu, T., Hu, Z., Zhou, C., Shi, P., Zhang, T., 2020. Identification and expression characterization of a novel carboxypeptidase A-like gene (RvCPA) during early developmental stages in the gastropod Rapana venosa (Muricidae). Aquaculture Reports 17, 100360. https://doi.org/10.1016/j.aqrep.2020.100360

Young, T., Kesarcodi-Watson, A., Alfaro, A.C., Merien, F., Nguyen, T.V., Mae, H., Le, D.V., Villas-Bôas, S., 2017. Differential expression of novel metabolic and immunological biomarkers in oysters challenged with a virulent strain of OsHV-1. Dev. Comp. Immunol. 73, 229–245. https://doi.org/10.1016/j.dci.2017.03.025

Zacchi, L.F., Selmecki, A.M., Berman, J., Davis, D.A., 2010. Low Dosage of Histone H4 Leads to Growth Defects and Morphological Changes in Candida albicans. PLoS ONE 5, e10629. https://doi.org/10.1371/journal.pone.0010629

Zhang, Guofan, Fang, X., Guo, X., Li, L., Luo, R., Xu, F., Yang, P., Zhang, L., Wang, X., Qi, H., Xiong, Z., Que, H., Xie, Y., Holland, P.W.H., Paps, J., Zhu, Y., Wu, F., Chen, Y., Wang, Jiafeng, Peng, C., Meng, J., Yang, L., Liu, J., Wen, B., Zhang, N., Huang, Z., Zhu, Q., Feng, Y., Mount, A., Hedgecock, D., Xu, Z., Liu, Y., Domazet-Lošo, T., Du, Y., Sun, X., Zhang, Shoudu, Liu, B., Cheng, P., Jiang, X., Li, J., Fan, D., Wang, W., Fu, W., Wang, T., Wang, B., Zhang, J., Peng, Z., Li, Yingxiang, Li, Na, Wang, Jinpeng, Chen, M., He, Y., Tan, F., Song, X., Zheng, Q., Huang, R., Yang, Hailong, Du, X., Chen, L., Yang, M., Gaffney, P.M., Wang, S., Luo, L., She, Z., Ming, Y., Huang, W., Zhang, Shu, Huang, B., Zhang, Y., Qu, T., Ni, P., Miao, G., Wang, Junyi, Wang, Q., Steinberg, C.E.W., Wang, H., Li, Ning, Qian, L., Zhang, Guojie, Li, Yingrui, Yang, Huanming, Liu, X., Wang, Jian, Yin, Y., Wang, Jun, 2012. The oyster genome reveals stress adaptation and complexity of shell formation. Nature 490, 49–54. https://doi.org/10.1038/nature11413

Zhang, G., Li, L., Meng, J., Qi, H., Qu, T., Xu, F., Zhang, L., 2016. Molecular Basis for Adaptation of Oysters to Stressful Marine Intertidal Environments. Annu Rev Anim Biosci 4, 357–381. https://doi.org/10.1146/annurev-animal-022114-110903

Journal Pre-proof

Highlights

The metabolism and immunity of oysters are modified as a function of their habitat.

Increasing oysters' bathymetry is an advantage against pathogens in the field.

An intertidal footprint in oysters is detected at the proteomic level.

Journal Pre-proof

Journal Pre-proof

Declaration of interests

☐ The authors declare that they have no known competing financial interests or personal relationships that could have appeared to influence the work reported in this paper.

☒ The authors declare the following financial interests/personal relationships which may be considered as potential competing interests:

Corporeau Charlotte reports financial support was provided by Ifremer Brittany Centre. Corporeau charlotte reports a relationship with IFREMER that includes: employment.

Journal Pre-proof